Nonlinear Inversion of 834 Å Airglow to Ionospheric O^+ Number Density

by

Jon F. Stinger

Submitted in Partial Fulfillment

of the Requirements for the Degree of

Master of Science in Mathematics with Operations Research Option

New Mexico Institute of Mining and Technology

Socorro, New Mexico

December 4, 1998

ACKNOWLEDGEMENT

I would like to thank Dr. Borchers, without whose constant attention this project would probably never have been finished. I would like to thank Dr. Thomas for all his help and support, and I would like to thank both Dr. Thomas and his associates at the NRL for the opportunity to be a part of this project. I would like to thank the rest of my committee, Dr. Hossain and Dr. Schaffer, for their help and support. I would like to thank the rest of the Math Department at New Mexico Tech for everything over the last couple of years. Finally, I would like to thank my family, friends, roommates, and others who have put up with me over the time that this project has occupied my existence, for being supporting and patient through the whole thing.

This thesis was typeset with LaTeX[1] by the author.

[1] LaTeX document preparation system was developed by Leslie Lamport as a special version of Donald Knuth's TeX program for computer typesetting. TeX is a trademark of the American Mathematical Society. The LaTeX macro package for the New Mexico Institute of Mining and Technology thesis format was adapted by Gerald Arnold from the LaTeX macro package for The University of Texas at Austin by Khe-Sing The.

ABSTRACT

Inverse methods are often required to solve geophysical problems in which we estimate real geophysical conditions from measurements taken from a remote sensor. Often, we can estimate what measurements would result from a given set of conditions using physical equations, or forward equations. Nearly as often, it is very difficult to solve the inverse of these physical equations. In these cases we are required to estimate the parameters of these forward equations by estimating and changing these parameters until we find a reasonable fit. To find a reasonable set of parameters, we use an inverse method such as the Levenberg-Marquardt method of least-squares parameter estimation. In this thesis, we use the Levenberg-Marquardt method to estimate O^+ number densities in the ionosphere given readings of 834 Å ultraviolet radiation taken from satellite instruments.

Table of Contents

List of Tables

List of Figures

Chapter 1

Introduction

Geophysical problems often require the use of inverse methods to find solutions. An inverse problem is a problem in which we know the outcome of readings taken from a sensor or set of sensors of some kind. What we are hoping to find, however, is the geophysical state which produces the readings obtained by the sensor.

We can physically develop an equation that will allow us to generate what readings will be produced from certain geophysical states. This is what is called a *forward problem*. A forward problem progresses directly forward in a physically logical way from initial physical conditions to results. That is, given a set of geophysical conditions, we can derive an equation that predicts the resulting readings from the sensor. The procedure for solving an inverse problem uses the procedure for solving the forward problem to determine the initial conditions.

We can often use optimization methods such as the Levenberg-Marquardt Method [Levenberg, 1944, Marquardt, 1963, Lawson and Hanson, 1974, Bard, 1974, Gill et al., 1981, Bevington and Robinson, 1992] with methods like Tikhonov Regularization [Tikhonov and Arsenin, 1977] to find the model that best estimates the retrieved data with respect to a least squared error fit. The best possible model would be geophysically feasible, and as simple as possi-

ble [Parker, 1994]. We find this best fit by minimizing χ^2, the sum of the squared errors between the set of retrieved data, d, and the data produced from our estimated parameters, $\bar{d}$, divided by the variance of each parameter, σ^2, as follows:

$$\chi^2 = \sum_{i=1}^{n} \frac{(\bar{d}_i - d_i)^2}{\sigma_i^2} \tag{1.1}$$

[Bevington and Robinson, 1992].

The geophysical problem of interest is the determination of the O^+ ion *number density*, or atoms per unit volume, in the F layer of the ionosphere. The F layer of the ionosphere is between the altitudes of 150 and 1100 kilometers. This measurement is made at a spacecraft by the reception of 834 Å radiation in the ultraviolet portion of the electromagnetic spectrum. A number of upcoming satellite projects will gather 834 Å airglow data in the interest of modelling the O^+ number density in the F layer of the ionosphere. These projects include the Remote Atmospheric And Ionospheric Detection System (RAIDS) [Christiansen et al., 1993] and the Special Sensor Ultraviolet Limb Imager (SSULI) [McCoy et al., 1994].

When solar radiation strikes an oxygen atom in and below the F layer of the ionosphere, the molecule absorbs enough energy to allow the oxygen to ionize. In the ionization process, an electron is released, along with a photon at 834 Å. These photons are of a wavelength to allow *multiple resonant scattering*. Multiple resonant scattering is the absorbtion and reemission of photons by atoms, which changes the direction of motion for the said photon. This means that all photons moving along a specific line of sight were not necessarily originally emitted from O^+ ions along that line of sight[Picone et al., 1997, McCoy et al., 1985]. Additionally, other ions and molecules in the ionosphere

can simply absorb free photons. These factors complicate the determination of O^+ number density from 834 Å ultraviolet radiation intensity [Picone et al., 1997]. These satellites will use a technique called *limb-scanning*. Limb-scanning is a process in which measurements are taken at many altitudes in the F layer, by varying the angle at which the sensor looks. The angles of these measurements range from skimming the very top of the ionosphere to pointing vertically into the ionosphere. Data over multiple angles allow for estimations to be made for multiple layers of the ionosphere. A first reading would find an intensity for only the very top 'layer' of the ionosphere. A second reading, with an angle penetrating into more of the ionosphere, would find an intensity reading due to two layers, including the first. Measurement at a number of angles, then, gives us intensities due to many layers of the ionosphere. These data would be produced from a set of specific O^+ number densities in the forward model. We can therefore use these readings in an inverse model to find a good model set of number densities that would produce given readings.

A forward model that translates O^+ number densities in the ionosphere to 834 Å ultraviolet intensity is necessary to solve the desired inverse problem. To solve the forward problem, we need to know the conditions in the ionosphere at the time the measurements were taken. These conditions include the concentrations of other molecules and atoms (N_2, O_2, N, He, O, H, and Ar), and temperature. For the generation of this data, and data in previous research [Picone et al., 1997] we use the mass spectrometer incoherent scatter 1986 (MSIS-86) model [Hedin, 1987]. MSIS-86 generates this data from information including: year, day, latitude, longitude, universal time, solar zenith angle, and solar 10.7-cm flux from the previous day and averaged over the pre-

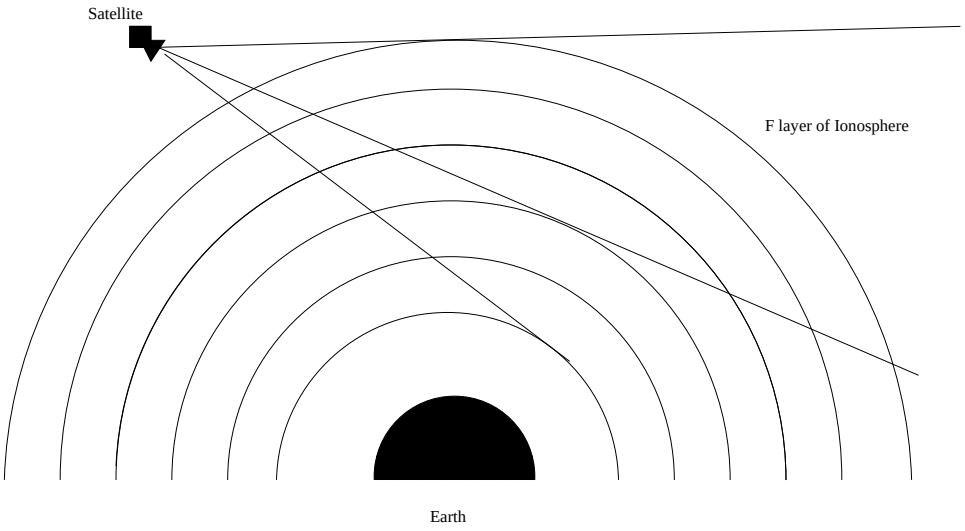

Figure 1.1: Diagram of Limb Scanning of the F Layer of the Ionosphere Separated into Layers

vious 81 days. These values are found separately at the time of the satellite readings and are used in the MSIS-86 process as constants.

[Picone et al., 1997] modelled the O^+ number density of the F layer of the ionosphere using the Levenberg-Marquardt method for nonlinear least squares problems in 1997. The satellite data would be used to fit a four parameter equation that modelled observed ionospheric data, the four-parameter Chapman equation [Anderson and Meyer, 1985]. The four parameters coincide with: the altitude of maximum number density, the number density at that altitude, and two parameters that control the drop-off rates of the number density as altitude varies. These four parameters, given satellite data, are estimated using the Levenberg-Marquardt method. Unfortunately, the Chapman equation, while it accurately models most currently available ionospheric O^+ number density, does not work well in all cases and may reject interesting features. It

would, therefore, be beneficial to have an inverse procedure that does not use the Chapman equation.

There are other models that are used for estimating O^+ concentrations in the ionosphere, such as the parameterized ionospheric model (PIM). This ionospheric model does not use the four-parameter Chapman equation, but instead forms data sets from theoretical equations based on parameters including magnetic activity, interplanetary magnetic fields, 10.7-cm solar flux, season, and longitude [Daniell Jr. et al., 1995]. Like the Chapman equation, these parameters establish a profile over the F layer of the ionosphere.

The purpose of this thesis is to establish a means of determining the O^+ concentrations over the F layer of the ionosphere. This model should use only estimated concentrations at given altitudes with a cubic spline curve interpolating between those altitudes to make a fit to data from a satellite. This model would accomplish the goal of eschewing the Chapman equation, or any other profile-generating process, while creating a reasonable, smooth model of the F layer of the ionosphere.

While this model would be more acceptable in the field of ionospheric research, it is mathematically more complicated because of its ill-conditioned nature. An ill-conditioned problem is one in which small changes to values in the problem can cause large changes in the solution[Gill et al., 1981]. If we use the Levenberg-Marquardt method by itself in this and other ill-conditioned problems, the resulting solution set is rough, increasing and decreasing erratically. This erratic model is physically unreasonable. The layer parameters should be smooth, increasing quickly and evenly then decreasing more slowly as we rise through the given altitudes. To find a smooth solution to this inverse prob-

lem using the Levenberg-Marquardt method requires the use of regularization, which will smooth the solution, making it physically reasonable. In this case, Tikhonov regularization is used to smooth the solution.

The problem of uniqueness arises in inverse theory. When using parameters to generate a model to represent the retrieved data, we can possibly get an infinite number of solutions. Is there a unique solution? To find a solution to the problem of parameter fitting, we minimize an objective function based on finding a good fit to the retrieved data. We know that there is noise in the retrieved data, so we do not wish to match it exactly. What we wish to do is find a smooth function that minimizes the sum of squared errors between the retrieved data and the fitted data. If we are regularizing, we minimize the sum of squared errors plus the regularization term. We have uniqueness because this minimum is the fit that best minimizes this objective function.

Chapter 2

Nonlinear Inverse Methods

2.1 Levenberg-Marquardt Method of Nonlinear Least Squares Parameter Estimation

When solving a nonlinear inverse problem, it is often desirable to minimize a function which is the sum of the squared errors between the values of the retrieved data and the values of the data resulting from the chosen parameters in the forward problem. The Levenberg-Marquardt method is a least-squares method of parameter estimation for nonlinear problems. It is an iterative method in which we use an initial estimated set of model parameters to generate a final set of model parameters that minimizes the sum of squared errors between itself and the data set retrieved from research.

These methods take advantage of the fact that residual errors for a number of data points of a function have some interesting and useful properties. Given residual errors between the retrieved data set,$\bar{d}$, and the data set derived from initial guess parameters,d, $(\bar{d}_i - d_i)$, and the variance of each of those data points σ_i one half of the sum of the squares of those errors is equal to the function $F(x)$:

$$F(x) = \frac{1}{2}\sum_{i=1}^{n}\frac{(\bar{d}_i - d_i)^2}{\sigma_i^2} = \frac{1}{2}\|\frac{\bar{d} - d}{\sigma}\|_2^2. \tag{2.1}$$

If f is the current set of estimated forward model solution data, the gradient of $F(x)$ is

$$\nabla F(x) = J(x)^T f(x) \tag{2.2}$$

and the Hessian is

$$\nabla^2 F(x) = J(x)^T J(x) + Q(x) \tag{2.3}$$

where $J(x)$ is the Jacobian of $f(x)$, and

$$Q(x) = \sum_{i=1}^{m} f_i(x) \nabla^2 F(x) \tag{2.4}$$

[Gill et al., 1981].

The Levenberg-Marquardt method takes advantage of two parameter estimation techniques: the steepest descent method and the Gauss-Newton method. Both of these methods have inadequacies that are resolved by the Levenberg-Marquardt method. The steepest descent method of parameter estimation will converge to a minimum, but does so very slowly. The Gauss-Newton method has the opposite problem. It generally converges quickly, but sometimes fails to converge at all. The Levenberg-Marquardt method, therefore, uses steepest descent while the estimated parameter set is far from the best fitting parameter set, and the Gauss-Newton method when the parameter set is very close to the best fitting parameter set. In between, Levenberg-Marquardt uses a mixture of both processes [Bevington and Robinson, 1992].

2.1.1 The Steepest Descent Method

The steepest descent method, also known as the gradient search method, uses the negative of the gradient of the forward problem, $-\nabla F(p)$ at the set of estimated parameters p, the direction of steepest descent, to find a direction to search. The gradient can be estimated by finite differences or by using the derivatives of the forward model with respect to the parameters if formulas for

the derivative are available. The negative gradient can then be multiplied by a positive step length scalar constant α to produce a vector Δp, which is added to p to form a new set of parameters, and the process is repeated. This step can be summarized in the equation

$$\Delta p = -\nabla F(p)\alpha \tag{2.5}$$

$$p + \Delta p \rightarrow p_{new} \tag{2.6}$$

[Gill et al., 1981, Bevington and Robinson, 1992].

As mentioned, the problem with the steepest descent method is its slow convergence rate. As we approach the set of parameters which gives a minimum sum of squared errors when compared to the retrieved data set, the gradient approaches zero. The change in the parameters at these values therefore also approaches zero. At values close to the minimum, we get gradient vectors that go one way, then another as we fine-tune towards the minimum. At values close to the correct minimum, we therefore get very slow convergence. The steepest descent method converges linearly, and in practice, this linear convergence is *very* slow [Gill et al., 1981, Bevington and Robinson, 1992].

2.1.2 The Gauss-Newton Method

Newton's method uses the Taylor series approximation of the forward model taken to the second derivative to find a step length and direction for the parameter values p. The Taylor series expansion to the second derivative term of the forward model is

$$F(x + \Delta x) \approx F(x) + \nabla F(x)^T \Delta x + \frac{1}{2}\Delta x^T \nabla^2 F(x) \Delta x. \tag{2.7}$$

To minimize any given function $\Phi(x)$, we want its derivative $\nabla\Phi(x) = 0$. So the minimum of the above expansion equation with respect to Δx occurs when its derivative with respect to Δx is equal to zero:

$$\nabla F(x) + \nabla^2 F(x)\Delta x = 0. \tag{2.8}$$

We can see that we get a minimum when

$$\nabla^2 F(x)\Delta x = -\nabla F(x) \tag{2.9}$$

[Gill et al., 1981, Bard, 1974, Bevington and Robinson, 1992].
Examining this equation and using the above theory on least squares problems, we can derive the Gauss-Newton method of linear least squares parameter estimation, where Δp is the step length taken on our guessed parameters that will minimize the residuals, $F(p)$.

$$(J(x)^T J(x) + Q(x))\Delta p = -J(x)^T f(x). \tag{2.10}$$

We can in practice ignore the $Q(x)$ in the function, as $J(x)^T J(x)$ tends to dominate the equation. If we remove $Q(x)$ from the equation, we can still get a good answer reasonably quickly under most conditions. This makes it unnecessary to compute second derivatives. After dropping the $Q(x)$, we get the Gauss-Newton method, which uses the equation

$$(J(x)^T J(x))\Delta p = -J(x)^T f(x) \tag{2.11}$$

[Gill et al., 1981].

2.1.3 The Levenberg-Marquardt Method

A problem with the Gauss-Newton method occurs when the $J(p)^T J(p)$ matrix is ill-conditioned. We need a well-conditioned $J(p)^T J(p)$ matrix of full rank because in the course of solving the equation

$$p = ((J(p)^T J(p))^{-1}(-J(p)^T f(p)) \tag{2.12}$$

we must factor the matrix. A poorly conditioned matrix can be impossible to factor on a computer, as round-off can make it rank deficient. Ill conditioning, though, occurs all too often in nonlinear inverse problems[Gill et al., 1981]. We can make this matrix positive definite, and therefore Cholesky factorizable, by adding an identity matrix multiplied by a variable element λ which is large enough to make the matrix eigenvalues strictly positive. This gives a final equation of

$$(J(p)^T J(p) + \lambda I)\Delta p = -J(p)^T f(p). \tag{2.13}$$

This equation gives us a good balance between steepest descent and Gauss-Newton. If the $J(p)^T J(p)$ matrix can handle a small lambda, the Levenberg-Marquardt step is effectively a Gauss-Newton step, because λI can be negligible. If λ is large enough to make the $J(p)^T J(p)$ inconsequential in relation to the λI, the step is effectively

$$\lambda \Delta p = -J(p)^T f(p) \tag{2.14}$$

a steepest descent step since it is equivalent to

$$\frac{1}{\alpha}\Delta p = -\nabla F(p) \tag{2.15}$$

where α is a scalar constant, as we have already stated that $-J(p)^T f(p) = -\nabla F(p)$ [Gill et al., 1981].

We therefore need a method of establishing the value of λ for a given step. A simple scheme for choosing λ is as follows:

1): Let $\nu > 1$.

2): Set $\lambda^{(0)}$ to a small value, like 10^{-4}.

3): Compute Δp and $F(p + \Delta p)$ using this λ.

4): If $F(p + \Delta p) > F(p)$, increase λ by a factor of ν and repeat.

5): If $F(p + \Delta p) < F(p)$, decrease λ by a factor of ν, set $p' = (p + \Delta p)$ and repeat 4, using p' for p

[Marquardt, 1963, Bevington and Robinson, 1992].

By repeating this method over multiple iterations, and changing p to $p + \Delta p$ only if the step is a relative improvement, we can eventually reach an optimal solution for the parameters of the data-producing equation given the initial data set. It is possible to reach a local minimum, so a good selection of initial guess parameters is necessary [Gill et al., 1981].

2.2 Tikhonov Regularization

A regularization process is a process that is used to choose a solution that is reasonable for the intended process [Lawson and Hanson, 1974, Tikhonov and Arsenin, 1977, Tikhonov et al., 1995]. In the case of this and

many other processes, reasonable can be defined as smooth with regard to the second derivative of the function. As we do not get an explicit function from an inverse model such as our spline fit model, we must utilize a regularization procedure that uses the information we do have on the inverse model.

Tikhonov regularization is the procedure we use for the process of smoothing the inverse model with respect to its second derivative. In the process of Tikhonov regularization, we minimize the sum of two quantities: the squared errors between the retrieved data and the produced inverse model, $F(p) - d$, as we would in least squares methods such as the Levenberg-Marquardt method; and the 2-norm of the vector to be regularized, z, times a constant *regularization parameter* μ. In essence, we minimize the function

$$\|F(p) - d\|^2 + \mu\|z\|^2 \tag{2.16}$$

[Tikhonov and Arsenin, 1977, Tikhonov et al., 1995].

In the case of our problem, we wish to regularize the second derivative of the inverse model, so we need to alter the vector to be regularized. To regularize the second derivative of the function, we may multiply the parameters of the inverse problem, p, by the matrix L, the matrix of sums of squares of the second differences:

$$\begin{bmatrix} -1 & 2 & -1 & 0 & 0 & \cdots & 0 \\ 0 & -1 & 2 & -1 & 0 & \cdots & 0 \\ 0 & 0 & -1 & 2 & -1 & \cdots & 0 \\ \vdots & \vdots & \vdots & \vdots & \vdots & \ddots & \vdots \\ 0 & 0 & 0 & \cdots & -1 & 2 & -1 \end{bmatrix}$$

as Lp.[Twomey, 1977]. We may then restate the equation to be minimized as

$$\|F(p) - d\|^2 + \mu\|Lp\|^2. \tag{2.17}$$

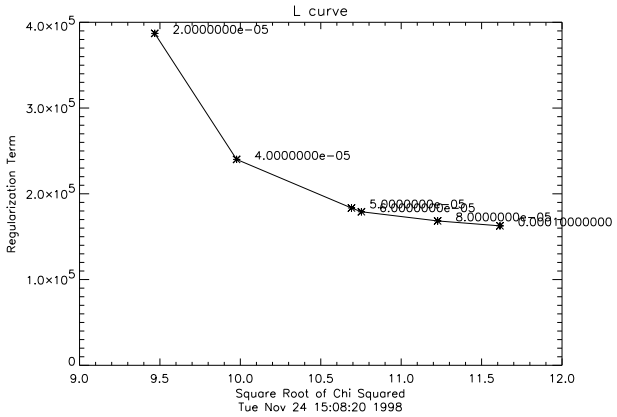

Figure 2.1: Example L-Curve

This version of Tikhonov regularization compares the smoothness of the second derivatives of the inverse function to the least squares fit of the inverse function. The regularization parameter μ gives the regularization quantity of the minimization function the weight it needs. If more smoothness is necessary, raise the value of μ. If the smoothness should be less important than the value of the least squares fit, make μ smaller. It can be a very important decision to decide the value of a regularization μ.

2.3 The L-Curve

The L-curve is a graphical method of choosing the best value of the regularization parameter μ. The L-curve shows the tradeoff between the residual norm $\|F(p) - d\|_2$ on the x-axis and the regularization norm $\|Lp\|_2$ on the y-axis. We find an L-curve by plotting these two values for multiple runs of a regularization method using differing values for the regularization μ. These

points, if they include the optimal μ, will form an L shape, with the point corresponding to the optimal μ at the corner.

At the corner, we have a μ that finds the smallest value of $\|F(p) - d\|_2$ relative to the smallest $\|Lp\|_2$. The two errors are effectively balanced. If μ is any larger, we get an increasingly large final value $\|Lp\|_2$ while decreasing $\|Ap-d\|_2$ relatively little. Conversely, if μ is any smaller, we get an increasingly large $\|Ap - d\|_2$ while decreasing $\|Lp\|_2$ relatively little [Hansen, 1992].

Chapter 3

Inverse Model of O^+ Number Density Using the Chapman Equation

My inverse model of O^+ number density using the Chapman equation is based on, and is a recreation of, the model created by [Picone et al., 1997]. In many cases, this model works in the estimation of O^+ number density. In some cases, though, the Chapman equation fails to accurately model the O^+ number density.

We have tested the inverse model using the Chapman equation against two ionospheric models estimated from different sources: one created using the Chapman equation and one using PIM. These models are used in the absence of real, known ionospheric O^+ data with corresponding 834 Å readings. The Chapman equation and the PIM model estimate O^+ number density over the F layer of the ionosphere. These estimated models are then run through the forward model to produce 834 Å radiation data as it would be received by satellite instruments.

We have added random noise to the data produced by the forward models to make the estimated retrieved 834 Å data realistic. This random noise is based on an error equal to a normal random variable with a standard deviation equal to the square root of the estimated data point. This produces noise similar to real noise in real satellite data. This is true because the satellite instruments perform what is effectively a Poisson count of photons striking those instru-

ments. A Poisson distribution has a standard deviation σ equal to the square root of the mean μ, and can be acceptably estimated by a normal (or Gaussian) distribution for a significantly large μ [Bevington and Robinson, 1992].
When using the variables in the Chapman equation as parameters in our inverse model, no regularization is necessary, as all Chapman models are smooth curves.

3.1 Forward Model Using the Chapman Equation

The four-parameter Chapman equation [Anderson and Meyer, 1985] includes the following variables: the altitude of maximum number density z_{max}, the number density at that altitude N_{max}, and two parameters that control the drop-off rates of the number density as altitude varies, H_0 and H_1. These variables are used in the four-parameter Chapman equation

$$N_{O^+}(z) = N_{max}\exp\left[\frac{1}{2}\left(1 - \frac{z - z_{max}}{H_0 + H_1 z} - \exp\left[-\frac{z - z_{max}}{H_0 + H_1 z}\right]\right)\right] \tag{3.1}$$

to evaluate a number density N_{O^+} at altitudes z over the F layer of the ionosphere.
For purposes of the inverse procedure, we scale all of these parameters. This scaling lowers the ill-conditioning of the Jacobian matrix by setting all of these values to be on the order of one. In this scaling, we use parameters that are on the order of one, and multiply them by the factors in Table 3.1 before applying them to the Chapman equation.

This equation is the function of a curve that estimates O^+ number density over the F layer of the ionosphere. We use fifty points along this curve, at

Table 3.1: Multiplication Factors of Parameters in Chapman Equation

Parameter	Multiplication Factor
N_{max}	10^5
z_{max}	10^2
H_0	10^1
H_1	10^{-2}

20 km intervals over the F layer, as a discrete estimation of this curve. We then use this discrete estimation of the O^+ number densities over the F layer in our forward model to evaluate the 834 Å radiation readings expected from our satellite sensors. The forward model [Picone et al., 1997] is the following series of equations

$$j(z) = j_0(z) + \sigma_0 N_{O^+}(z) \int_{z_0}^{\infty} j(z') H(|\tau' - \tau|, |t' - t|) dz' \tag{3.2}$$

which evaluates the volume emission rate $j(z)$ for 834 Å given the definitions for the constants as given in Table 3.2 and the MSIS-86 paramenters given in Table 3.3.

Given this data, the volume excitation rate $j(z)$, we must then perform the integration to estimate the column emission rate $4\pi I$, where I is the radiance in megaphoton cm^{-2} sec^{-1} $ster^{-1}$ as measured at the satellite:

$$4\pi I(\mathbf{r}, \hat{\mathbf{e}}) = 10^{-6} \int j[\mathbf{r}'(s)] T(\mathbf{r}', \mathbf{r}) ds \tag{3.3}$$

given the constants defined in Table 3.4.

These integrals are discretized and evaluated numerically in code developed for [Picone et al., 1997]. The result is an array of ninety retrieved 834 Å intensities over varying limb-scan angles.

Table 3.2: Constants Used in Forward Model Equation 1

$j_0(z)$	the initial photon production term – provided by certain databases
z_0	altitude below which the initial photon term is negligible or extinction is large
σ_0	resonant scattering line-center cross section for 834 Å radiation
$\tau(z)$	the vertical resonant scattering line-center optical depth at altitude z
$t(z)$	the vertical pure absorbtion optical depth at altitude z
H	the Holstein probability function, which is the transport kernal, proportional to the probability that a photon propagates from one region $(z', z' + dz')$ to another region $(z, z + dz)$.

Table 3.3: Constants Used in the MSIS-86 Process Used in the Forward Model

latitude	=	10°
longitude	=	60°
local time	=	10 hours
day	=	133
year	=	1988
satellite altitude	=	832 km
satellite inclination angle	=	67.0°

Table 3.4: Constants Used in Forward Model Equation 2

$\hat{\mathbf{e}}$	the line of sight of the satellite instrument
$\mathbf{r}'$	the initial location of the photon
$\mathbf{r}$	the location of the satellite instrument
T	the probability that a photon travelling along $\hat{\mathbf{e}}$ from $\mathbf{r}'$ will arrive at $\mathbf{r}$.

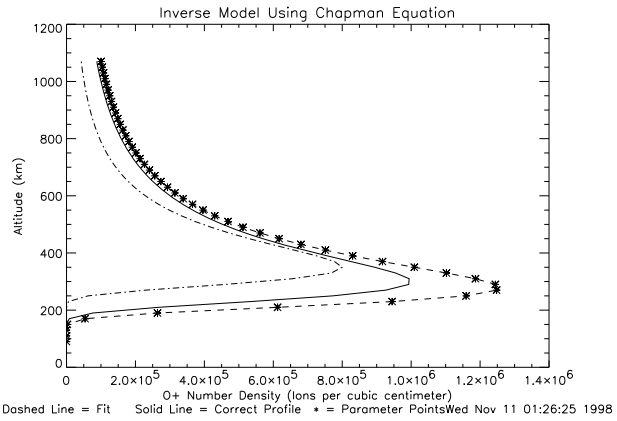

Figure 3.1: Chapman-Generated O^+ Concentration in the F Layer of the Ionosphere and the Chapman Equation Inverse Solution

3.2 Chapman Inverse Model Using an Initial Ionospheric Model Estimated from the Chapman Equation

We first used the Chapman equation inverse model to find a solution to a data set created by using the Chapman equation itself. The unscaled parameters of the Chapman equation were

$$[z_{max}, N_{max}, H_0, H_1] = [300, 10^6, 35, .09].$$

Our Chapman equation-based Levenberg-Marquardt program found a solution of

$$[z_{max}, N_{max}, H_0, H_1] = [278, 1.26 \times 10^6, 32.5, .0918].$$

These parameters produce a plot that compares to the original as shown in Figure 3.1.

This set of Chapman parameters produces a set of 834 Å satellite readings that matches the initial set of noisy data as shown in Figure 3.2. The Chi-squared value of this fit is 81.787 over 86 degrees of freedom, which produces a one-sided

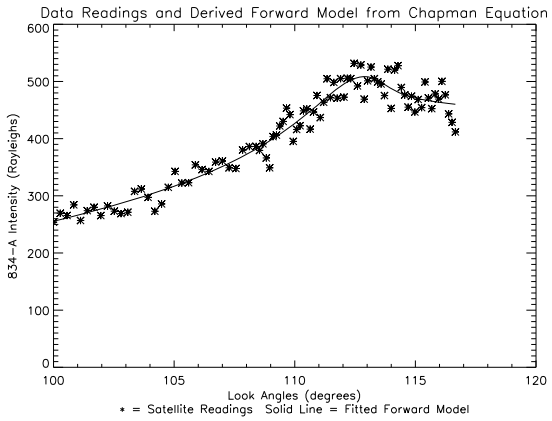

Figure 3.2: Chapman-Generated Forward Fit 834 Å Intensity Data and Noisy Chapman Equation Produced Data

p-value of .3914 [Bain and Engelhardt, 1992]. This p-value is the probability that χ^2 would be so large if the fit were correct. A p-value of .3914 means that we have a .3914 probability that we would get residuals like this if this was our initial data set. A p-value of .05 or less would mean that the fit was poor.

We can also plot the standardized residuals of the forward model from our fit to the retrieved data. This plot will show us that a good fit exists if the residuals appear to be normally distributed. Standardized residuals are the difference between the retrieved data points and the fitted data divided by the estimated standard deviation of the readings σ. In this case the standard deviation is the square root of the retrieved data. The method of determining a standardized residual for a fit is as follows:

$$SR_i = \frac{\bar{d}_i - d_i}{\sigma_i}. \tag{3.4}$$

A normally distributed set of standardized residuals would have the most values near the mean, or zero standard deviations. As we move out from the

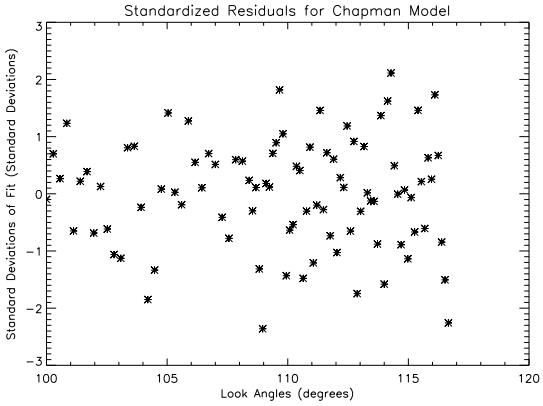

Figure 3.3: Standardized Residuals of the Chapman Equation Fit to Chapman Equation Generated Retrieval Data

mean, the density of standardized residuals occurring would get smaller, until only a few values go as far as the third standard deviation. Figure 3.3 shows the standardized residuals of the Chapman equation fit of the data set generated from the Chapman equation. We also look for patterns in the residuals, such as strings of sequential residuals with positive standardized residuals [Ramsey and Schafer, 1997].

We may examine the standardized residuals in Figure 3.3 and the regression fit of these residuals in Figure 3.5 and note that no patterns or trends appear. We can go farther in testing the normality of the residuals by producing a *normal probability plot*, or Q-Q Plot. This plot is a visual aid to show normality. If the plot is normal, the points will appear in a fairly straight diagonal line, grouped together near the center and spread out more at the ends. If there are curves in the plot, then the residuals are not normally distributed. We show the normal probability plot for the fit to the Chapman data set in Figure 3.4. We can see from the p-value of the Anderson-Darling test that we have a

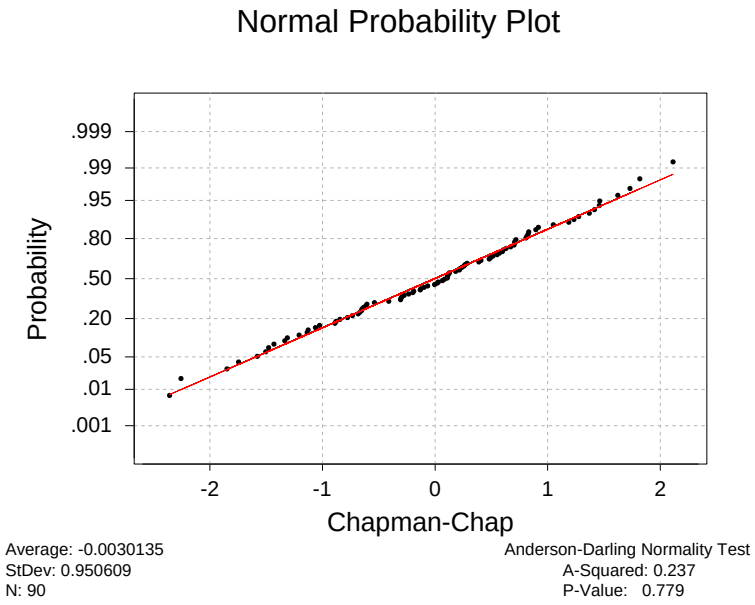

Figure 3.4: Anderson-Darling Normal Probability Plot for Chapman Fit to Chapman Data

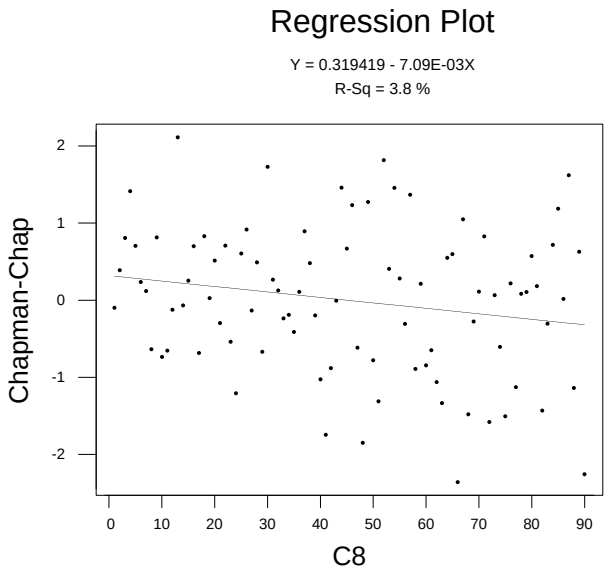

Figure 3.5: Regression of Residuals in Chapman to Chapman Fit

reasonably normal distribution of residuals [D'Augostino and Stevens, 1986]. Having established that we have made a reasonable fit with respect to having normal residuals, we now must establish the likely range of the Chapman parameters. The parameters we have fit to the model are only estimates. We need to know how certain we are with the fit. To show this certainty in the range of each parameter, we must produce a covariance matrix [Bain and Engelhardt, 1992]. A covariance matrix is a square, symmetric matrix with a number of diagonal elements equal to the number of parameters. Each diagonal element is the variance, σ^2, of the respective parameter. Each nondiagonal element is the covariance of the two elements that coincide with its row and column. The covariance matrix established from the Levenberg-Marquardt method is equal to $(J^T J)^{-1}$, where J is the Jacobian of the final iteration of the Levenberg-Marquardt process. The covariance matrix for the Chapman fit of the scaled parameters of the Chapman-generated data is

$$\begin{bmatrix} 0.05447 & -0.91449 & -0.17871 & 0.32398 \\ -0.91449 & 15.651 & 3.4324 & -5.9747 \\ -0.17871 & 3.4324 & 4.9679 & -6.5320 \\ 0.32398 & -5.9747 & -6.5320 & 8.8418 \end{bmatrix}.$$

We can use the covariance matrix to generate a correlation matrix. A correlation matrix is a covariance matrix with each row i of the matrix divided by the standard deviation of element i, σ_i and each column j of the matrix divided by the standard deviation of element j, σ_j. This gives a matrix with ones in the diagonal, and values between -1 and 1 for all nondiagonal elements. Each element shows the correlation between the parameters. A correlation of 1 means that the two elements have a directly proportional relationship. If one element increases, the other increases without changing the outcome. A correlation of

-1 means that the two elements have an inversely proportional relationship. One of the two elements decreases while the other increases, and the outcome will not change [Bain and Engelhardt, 1992]. This covariance matrix results in the following correlation matrix

$$\begin{bmatrix} 1 & -0.9904 & -0.3435 & 0.4668 \\ -0.9904 & 1 & 0.3893 & -0.5079 \\ -0.3435 & 0.3893 & 1 & -0.9856 \\ 0.4668 & -0.5079 & -0.9856 & 1 \end{bmatrix}.$$

This correlation matrix shows a strong inverse correlation between the first two parameters and between the last two parameters at the location of this solution. This means that one of the values in either pair can vary upward, and the other value in that pair can vary downward, and the value of the solution would change very little. This can cause a solution to result in a set of parameters different from the original parameter set by only one of the parameters varied up and the second in that pair varied down.

We can also use the covariance matrix to establish 95% confidence intervals for each parameter. A confidence interval is an interval of values which we are 95% confident that the correct answer lies within this interval [Bain and Engelhardt, 1992]. In the case of this solution, our 95% confidence interval, when we have unscaled the values from the covariance matrix, is

$$[z_{max}, N_{max}, H_0, H_1] = [278 \pm 46, 12.6 \times 10^5 \pm 7.87 \times 10^5, 32.5 \pm 44.35, .0918 \pm .0592].$$

We provide a sample of fits using the same initial parameters and differing noise in Tables 3.5 and 3.6 and Figures 3.6-3.14. These fits leave standardized residuals as shown in Figures 3.15-3.23.

The 95% Confidence Intervals for the parameters show the interval which is

Table 3.5: Chapman to Chapman Models Using Varying Noise Final Parameters

Data Set	z_{max} 95% CI	N_{max} 95% CI	H_0 95% CI	H_1 95% CI
1	[288.6,288.7]	[1307941,1328499]	[-2.418,-1.962]	[.1255,.1258]
2	[315.8,316.0]	[911161,920939]	[57.08,60.58]	[.0559,.0617]
3	[278.5,278.7]	[1224204,1286497]	[31.49,33.47]	[.0901,.0936]
4	[284.3,284.7]	[1200289,1353111]	[49.10,52.16]	[.0672,.0739]
5	[284.2,284.4]	[1117522,1147318]	[30.98,33.14]	[.0870,.0905]
6	[283.4,283.5]	[1159910,1181890]	[22.75,24.35]	[.0995,.1016]
7	[305.8,306.2]	[928559,957200]	[53.37,58.28]	[.0615,.0701]
8	[272.1,273.0]	[1154528,2166312]	[52.08,57.33]	[.0519,.0653]
9	[306.9,307.0]	[1009132,1017568]	[27.67,29.98]	[.0959,.0989]

95% likely to contain the correct value [Bain and Engelhardt, 1992]. The tests done in Table 3.6 show how good of a fit we have. The χ^2 and its p-value show the likelihood of having the resulting residuals if the fit is correct. A p-value of less than .05 means that we reject the hypothesis that this is a good fit.

The p-value for the Anderson-Darling test is the likelihood of having the resulting residuals if the distribution of residuals is normal. A p-value of less than .05 means the residuals are not normally distributed, and the fit is not good.

The last two columns on Table 3.6 are the 95% confidenct intervals of a linear regression fit to the standardized residuals. The parameters should both be zero. For a good set of residuals both confidence intervals would contain zero.

Table 3.5 shows that for z_{max}, we come close or cover the correct value of 300 with our confidence intervals. In six of the nine trials, the correct value is not included in the confidence interval. All other parameters are included in all confidence intervals over all trials.

Table 3.6 shows that the p-value of the fit for trial 9 is not good. Examining

Table 3.6: Chapman to Chapman Models Using Varying Noise Tests

	χ^2 Test		Regression of Residuals		
Data Set	χ^2	p-value	Anderson-Darling p-value	95% CI Regression Constant	95% CI Regression x-Coeff.
1	95.4934	.2269	.826	[-.5727,.3499]	[-.0131,.0045]
2	73.4577	.8304	.321	[-.1957,.7009]	[-.0149,.0022]
3	81.7870	.6086	.006	[-.8556,-.0751]	[.0029,.0177]
4	66.7124	.9389	.575	[-.8722,.0202]	[-.0004,.0167]
5	100.0304	.1430	.799	[-.1251,.6733]	[-.0117,.0035]
6	104.2095	.0883	.198	[.0302,.8648]	[-.0138,.0021]
7	94.0894	.2582	.359	[-1.083,-.1447]	[-.0005,.0174]
8	91.4632	.3232	.174	[-.2342,.5948]	[-.0033,.0105]
9	114.9792	.0201	.634	[-.7910,.0222]	[-.0003,.0152]

Figure 3.14 we can see that the fit appears to be good. In fact, Figure 3.14 appears to be quite possibly the best fit. But this trial is the only one which does not pass the χ^2 test. This shows that trusting the plot is not the appropriate way to test goodness-of-fit. We must use statistical tests to verify that the fit is good.

Trial 3 on Table 3.6 has a low Anderson-Darling p-value. This means that the distribution of residuals is not likely to be normal. This is not terribly surprising, as we have nine trials and the p-value is likely to be less than .05 even for good fits about 5% of the time. This trial is also flawed because neither regression coefficient confidence interval includes zero. Given this information, we are led to believe that the residuals are not only non-normal, but their mean is not zero, and they have a trend toward larger values as our look angle increases.

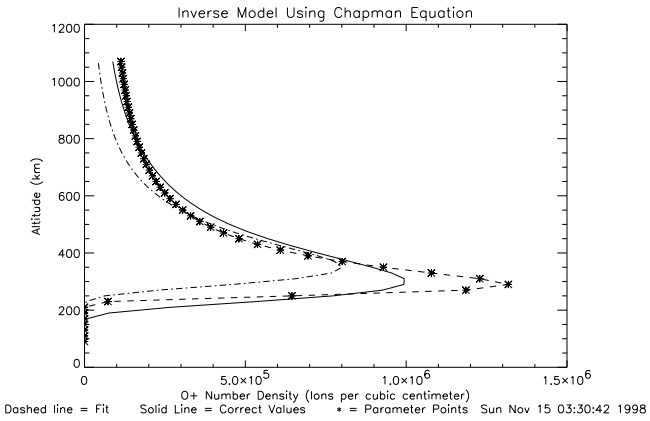

Figure 3.6: Chapman Equation Fitted to Chapman Data with Random Noise Set 1

We must also examine trials 6 and 7. Both of these trials are acceptably normal and have reasonable χ^2 values. But when we examine the residual regression fit, we see that the confidence interval for the constant does not include zero. The coefficient of x does include zero, so there is no statistically significant trend to the residuals. But the mean of the residuals is statistically not zero. This is not of as much concern as having a non-zero x-coefficent, but must be noted.

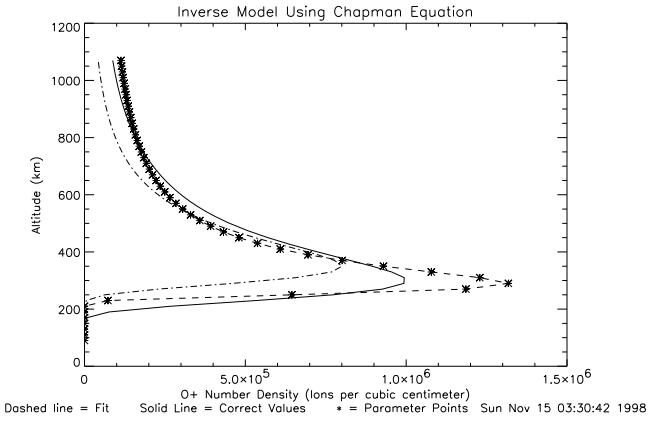

Figure 3.7: Chapman Equation Fitted to Chapman Data with Random Noise Set 2

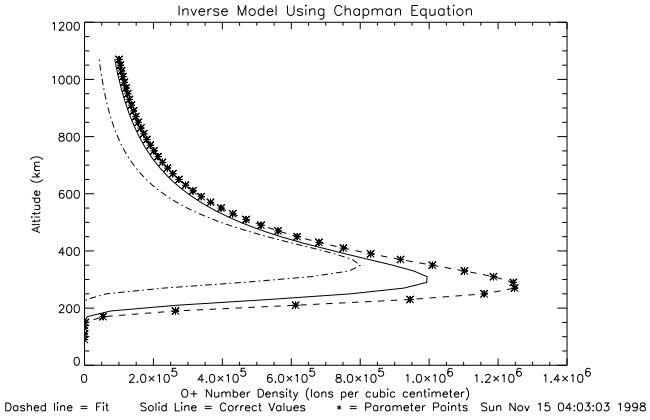

Figure 3.8: Chapman Equation Fitted to Chapman Data with Random Noise Set 3

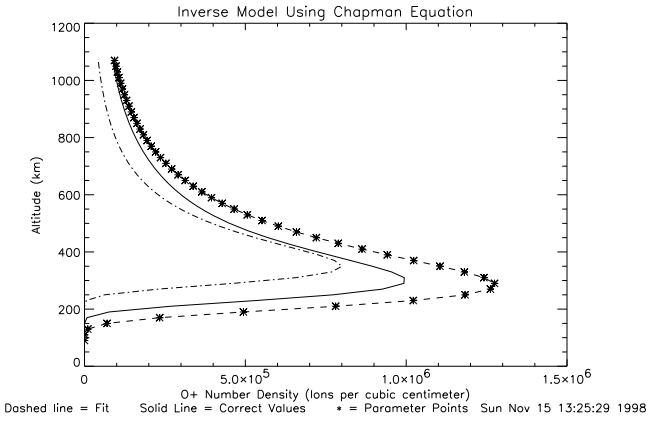

Figure 3.9: Chapman Equation Fitted to Chapman Data with Random Noise Set 4

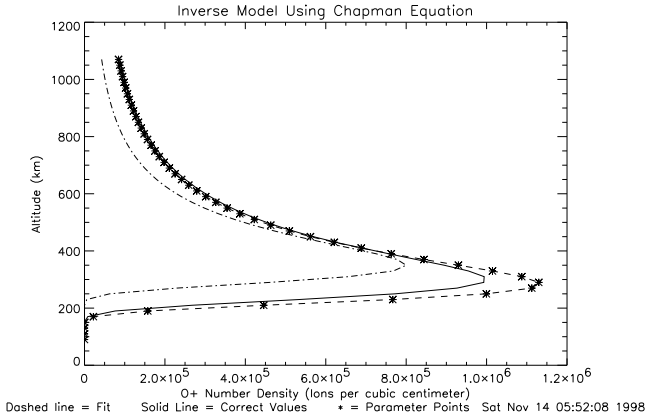

Figure 3.10: Chapman Equation Fitted to Chapman Data with Random Noise Set 5

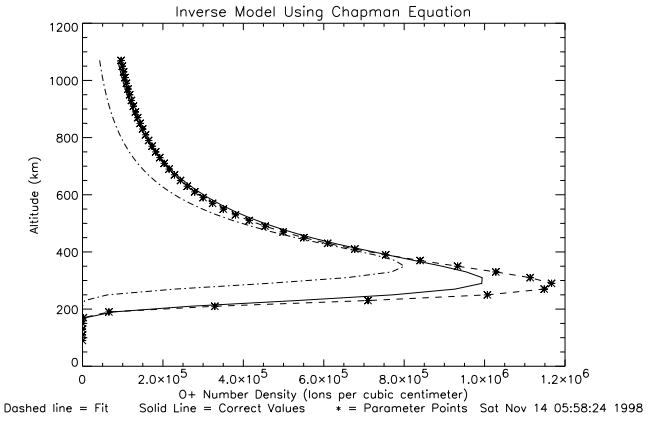

Figure 3.11: Chapman Equation Fitted to Chapman Data with Random Noise Set 6

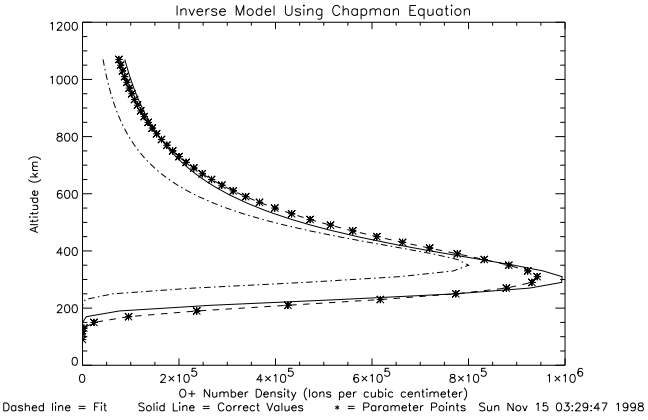

Figure 3.12: Chapman Equation Fitted to Chapman Data with Random Noise Set 7

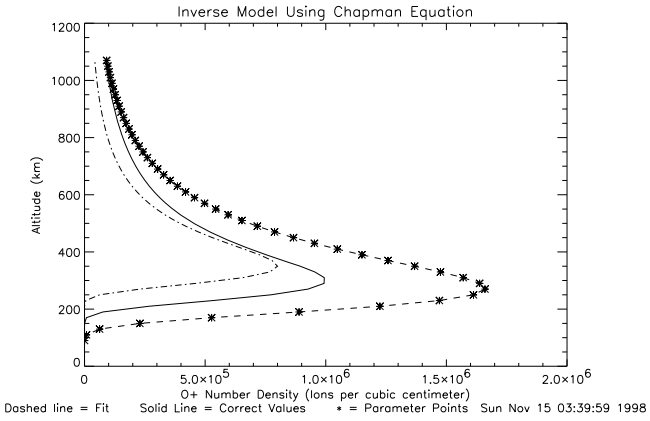

Figure 3.13: Chapman Equation Fitted to Chapman Data with Random Noise Set 8

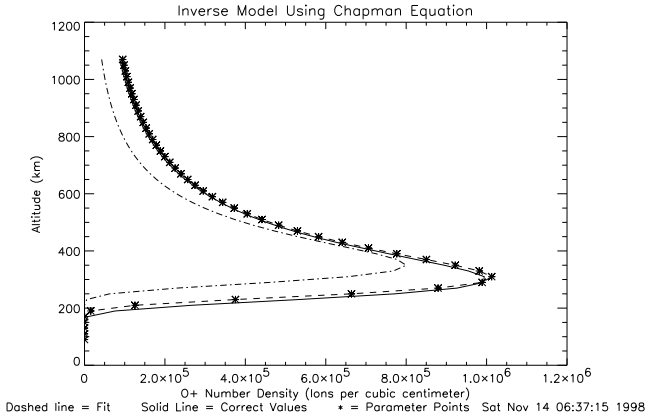

Figure 3.14: Chapman Equation Fitted to Chapman Data with Random Noise Set 9

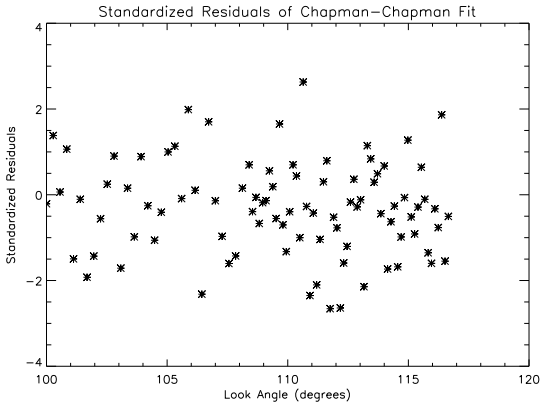

Figure 3.15: Chapman Equation Fitted to Chapman Data Standardized Residuals with Random Noise Set 1

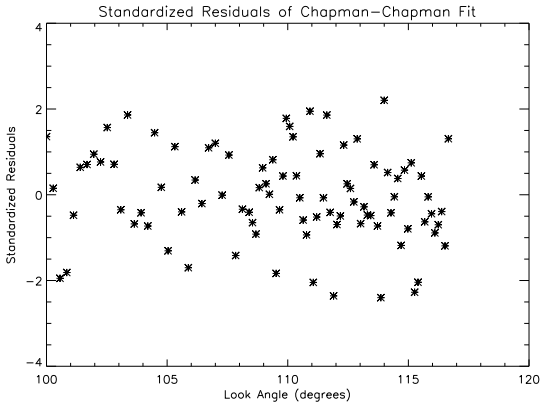

Figure 3.16: Chapman Equation Fitted to Chapman Data Standardized Residuals with Random Noise Set 2

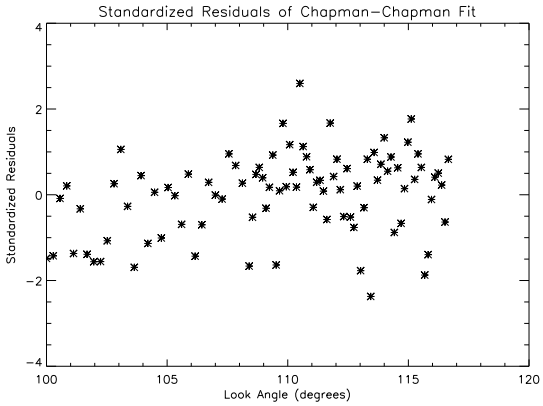

Figure 3.17: Chapman Equation Fitted to Chapman Data Standardized Residuals with Random Noise Set 3

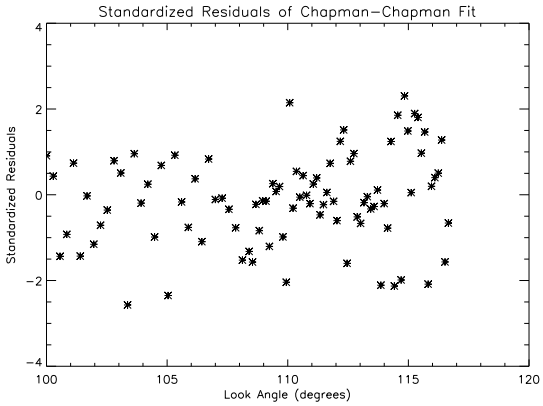

Figure 3.18: Chapman Equation Fitted to Chapman Data Standardized Residuals with Random Noise Set 4

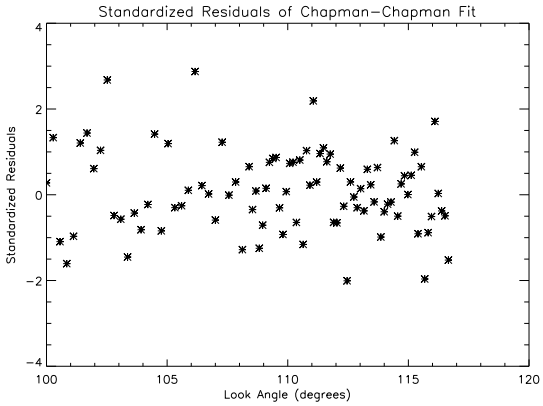

Figure 3.19: Chapman Equation Fitted to Chapman Data Standardized Residuals with Random Noise Set 5

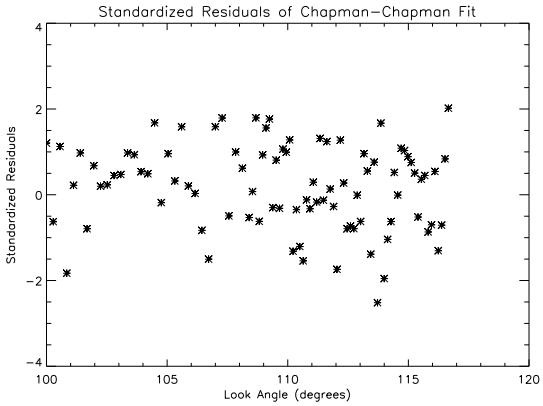

Figure 3.20: Chapman Equation Fitted to Chapman Data Standardized Residuals with Random Noise Set 6

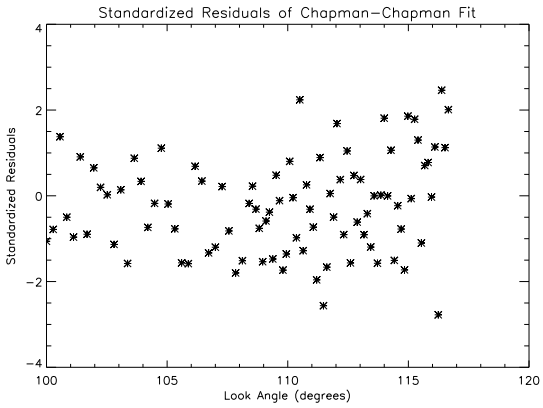

Figure 3.21: Chapman Equation Fitted to Chapman Data Standardized Residuals with Random Noise Set 7

3.3 Chapman Inverse Model Using an Initial Ionospheric Model Estimated from PIM

We next use the Chapman parameters to model a data set generated by a method that is not the Chapman equation. We use a set of O^+ number densities generated by the PIM model that are not easily modelled by the Chapman equation, as shown in Figure 3.24. The PIM values are the O^+ number densities over the altitudes of the F layer of the ionosphere.

After performing the Levenberg-Marquardt process on the initial guess parameters for the Chapman equation, we find that the unscaled Chapman equation fit parameters are

$$[z_{max}, N_{max}, H_0, H_1] = [358, 1.83 \times 10^6, 41.31, .1703].$$

These parameters result in the Chapman fit shown in Figure 3.24.

The final Chapman parameters produce a O^+ profile that results in a forward model fit shown in Figure 3.25, along with the noisy data produced from the PIM model. This model uses a standard deviation equal to the square root

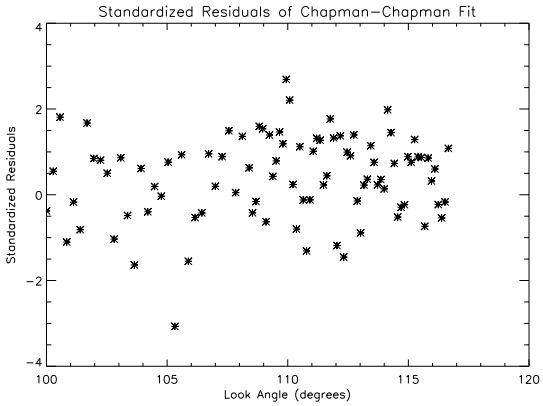

Figure 3.22: Chapman Equation Fitted to Chapman Data Standardized Residuals with Random Noise Set 8

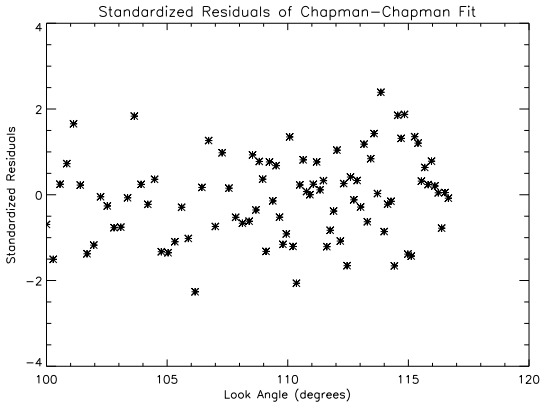

Figure 3.23: Chapman Equation Fitted to Chapman Data Standardized Residuals with Random Noise Set 9

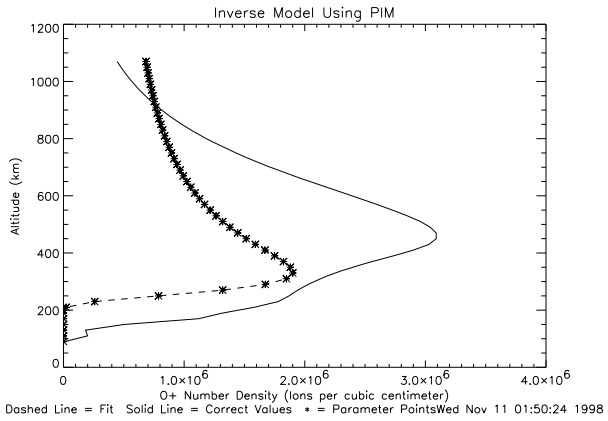

Figure 3.24: PIM-Generated O^+ Concentration in the F Layer of the Ionosphere and the Chapman Equation Inverse Solution

of each data point to represent instrument error, just as before. It appears that the fit is reasonably accurate, even though the fitted Chapman profile is nothing like the PIM profile.

To test the goodness of fit of our model of the data, we once again find a χ^2 value for the fit. The χ^2 in this case is 97.8591 for 86 degrees of freedom. This results in a p-value of .1798. This p-value tells us that we cannot reject the hypothesis that we have a good fit to the data.

We then check the standardized residuals for any patterns or deviations from normality. Looking at Figure 3.26, we see that the residuals appear to be normal. As another check of normality, we examine Figure 3.27 to test normality. The Anderson-Darling normal probability plot shows that the residuals are generally normal, with a p-value that does not reject the hypothesis of a good fit.

As we do not reject this model as a fit of the data, we then examine the covariance matrix. For the Chapman fit of the PIM-generated data set, we get

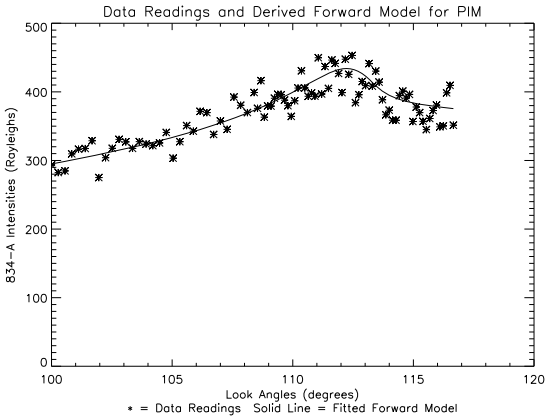

Figure 3.25: Chapman-Generated Forward Fit 834 Å Intensity Data and Noisy PIM Produced Data

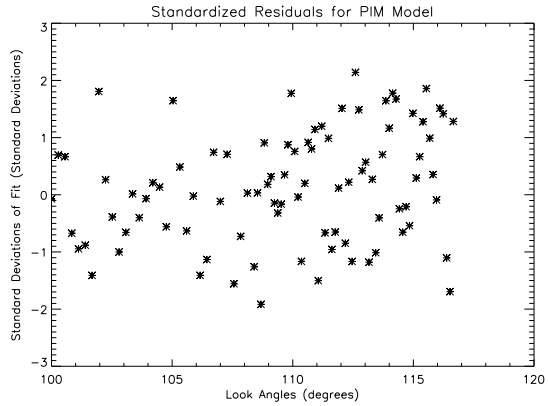

Figure 3.26: Standardized Residuals of the Chapman Equation Fit to PIM Generated Retrieval Data

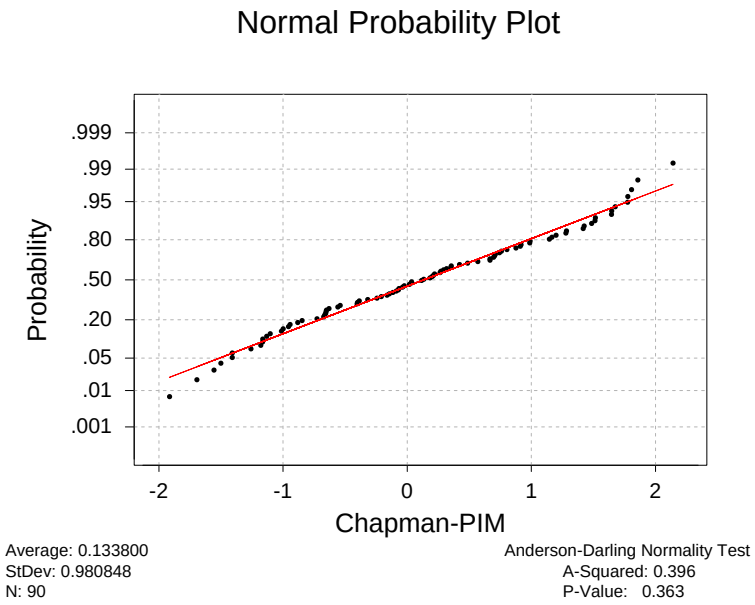

Figure 3.27: Anderson-Darling Normal Probability Plot for Chapman Fit to PIM Data

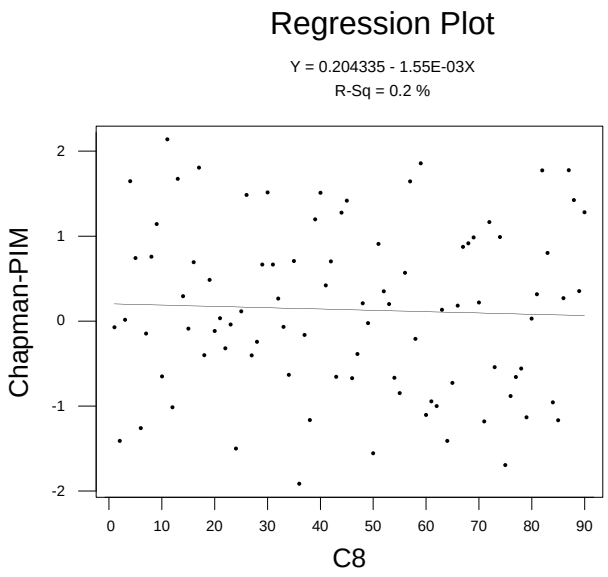

Figure 3.28: Regression of Residuals in Chapman to PIM Fit

a covariance matrix

$$\begin{bmatrix} 0.1907 & -0.2730 & 2.502 & -3.921 \\ -0.2730 & 11.766 & 8.706 & -10.268 \\ 2.502 & 8.706 & 47.19 & -71.54 \\ -3.921 & -10.268 & -71.54 & 112.768 \end{bmatrix}$$

for the scaled Chapman parameters. This covariance matrix results in a correlation matrix

$$\begin{bmatrix} 1 & -0.1823 & 0.8340 & -0.8455 \\ -0.1823 & 1 & 0.3695 & -0.2819 \\ 0.8340 & 0.3695 & 1 & -0.9807 \\ -0.8455 & -0.2819 & -0.9807 & 1 \end{bmatrix}.$$

These correlations show a correlation nearing -1 for the last two parameters. The last two parameters, therefore, are once again completely correlated, and can change, one up and one down, while changing the outcome very little.

When we use the covariance matrix to establish 95% confidence intervals for each parameter, we get the following results:

$$[z_{max}, N_{max}, H_0, H_1] = [358 \pm 86, 18.3 \times 10^5 \pm 6.8 \times 10^5, 41.31 \pm 136.7, .1703 \pm .2113].$$

We provide a sample of fits using the same initial parameters and differing noise in Tables 3.7 and 3.8 and Figures 3.29-3.37. These fits leave standardized residuals as shown in Figures 3.38-3.46.

From Figures 3.29-3.37, we can see that none of these gives us a very good estimation of the initial O^+ profile. But we have a decent χ^2 in most cases and pass all tests in some. We need to find a way to recognize a poor fit to the correct profile.

We contrast the previous tables and figures with Tables 3.9 and 3.10, and

Table 3.7: Chapman to PIM Models Using Varying Noise Final Parameters

Data Set	z_{max} 95% CI	N_{max} 95% CI	H_0 95% CI	H_1 95% CI
1	[356.6,357.4]	[1805200,1844000]	[30.61,47.35]	[.1540,.1918]
2	[445.6,446.2]	[1597200,1609400]	[98.87,144.73]	[.0168,.0613]
3	[375.6,376.6]	[1897400,2144800]	[47.44,79.98]	[.1082,.2029]
4	[402.1,403.1]	[1779300,2564100]	[63.55,113.59]	[.0560,.2148]
5	[366.7,367.5]	[1888000,2025800]	[50.62,72.70]	[.0992,.1535]
6	[362.0,363.0]	[1924900,2048900]	[39.47,65.37]	[.1218,.1884]
7	[384.0,385.4]	[1824700,1983500]	[50.69,88.53]	[.0948,.2037]
8	[410.8,411.8]	[1888500,1985700]	[70.16,100.60]	[.0646,.1565]
9	[410.1,411.3]	[1693300,1703100]	[51.77,78.39]	[.0976,.1744]

Figures 3.47-3.55. Figures 3.56-3.64 once again show residuals and any possible trends. These tables and figures give the results of the fitting of the same data with random noise with a standard deviation σ equal to one fourth the original noise.

In Table 3.8 we have little in the way of signals that we have a poor fit to the O^+ profile. Trial 9 fails to pass the χ^2 p test. Trials 1 and 4 fail the Anderson-Darling p-test, so we can believe that the residuals of those trials are not normally distributed. Trial 4 also has a constant regression of residuals parameter that is not statistically zero. We can see from Figures 3.29-3.37 that none of these trials produces a good fit. But only three fail any tests at all. These results are only slightly worse than the results of fitting to a Chapman profile in Table 3.6. The results of the tests of the fits shown in Figures 3.47-3.55 are much better at showing that these are not good fits. In Table 3.10, we see that trials 5, 6, 7, and 9 all fail the χ^2 test. Trials 1 and 8 are suspiciously close. Going to the Anderson-Darling p-test, we can now throw out trial 8 for

Table 3.8: Chapman to PIM Models Using Varying Noise Tests

	χ^2 Test		Regression of Residuals		
Data Set	χ^2	p-value	Anderson-Darling p-value	95% CI Regression Constant	95% CI Regression x-Coeff.
1	97.7828	.1812	.023	[-.3676,.3774]	[-.0106,.0037]
2	75.3653	.7869	.244	[-.2944,.5770]	[-.0095,.0072]
3	84.2469	.5333	.792	[-.8355,.1535]	[-.0019,.0170]
4	71.8355	.8631	.017	[-.9670,-.7115]	[.0035,.0206]
5	102.5184	.1081	.179	[-.1450,.8122]	[-.0162,.0021]
6	105.5880	.0745	.446	[-.3795,.5687]	[-.0055,.0090]
7	98.3354	.1712	.416	[-.8460,.0904]	[-.0029,.0150]
8	95.3887	.2291	.646	[-.2405,.7505]	[-.0114,.0075]
9	118.906	.0109	.410	[-.5934,.3048]	[-.0027,.0144]

Table 3.9: Chapman to PIM Models Using Varying Noise Final Parameters With A Quarter the Noise

Data Set	z_{max} 95% CI	N_{max} 95% CI	H_0 95% CI	H_1 95% CI
1	[408.37,408.43]	[1801700,1808100]	[93.22.95.06]	[.0801,.0852]
2	[438.58,438.62]	[1750000,1755200]	[120.36,121.48]	[.0269,.0302]
3	[421.06,421.14]	[1891900,1907500]	[111.56,114.02]	[.0493,.0563]
4	[427.47,427.53]	[1927000,1937800]	[117.94,119.99]	[.0421,.0478]
5	[418.37,418.45]	[1878600,1894000]	[111.33,113.64]	[.0441,.0504]
6	[416.25,416.32]	[1878200,1891500]	[107.22,109.60]	[.0540,.0604]
7	[429.37,429.43]	[1858900,1870700]	[120.07,121.97]	[.0344,.0397]
8	[429.96,430.02]	[1862200,1871000]	[116.10,117.77]	[.0399,.0448]
9	[435.11,435.19]	[1767700,1775300]	[115.39,117.45]	[.0373,.0427]

Table 3.10: Chapman to PIM Models Using Varying Noise Tests With A Quarter the Noise

	χ^2 Test		Regression of Residuals		
Data Set	χ^2	p-value	Anderson-Darling p-value	95% CI Regression Constant	95% CI Regression x-Coeff.
1	104.5696	.0845	.723	[-.6603,.2463]	[-.0086,.0087]
2	85.3472	.4996	.799	[-.6556,.2714]	[-.0048,.0129]
3	95.1040	.2353	.574	[-.5736,.1861]	[-.0034,.0111]
4	86.1200	.4761	.961	[-.6715,.1381]	[-.0043,.0111]
5	113.8272	.0240	.652	[-.6428,.2110]	[-.0058,.0105]
6	115.6160	.0183	.311	[-.2522,.5266]	[-.0093,.0056]
7	108.8896	.0484	.052	[-.5588,.2798]	[-.0053,.0107]
8	106.5808	.0656	.026	[-.2224,.6822]	[-.0108,.0064]
9	122.8624	.0056	.323	[-.6851,.2089]	[-.0033,.0137]

failing to be normal. We discard five of nine fits as poor fits, as opposed to three for full noise. A more sensitive instrument would allow us to determine poor fits more reliably.

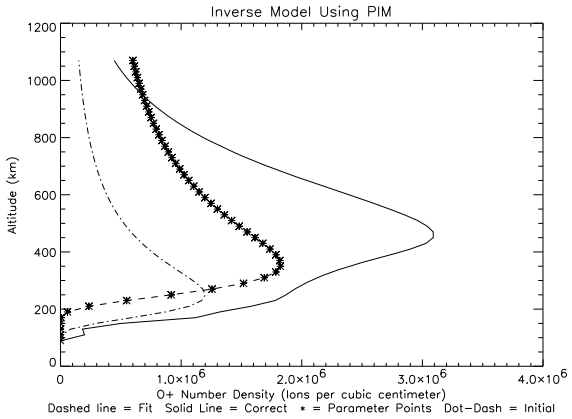

Figure 3.29: Chapman Equation Fitted to PIM Data with Random Noise Set 1

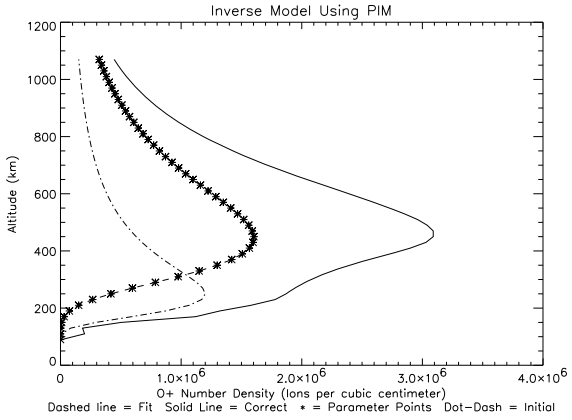

Figure 3.30: Chapman Equation Fitted to PIM Data with Random Noise Set 2

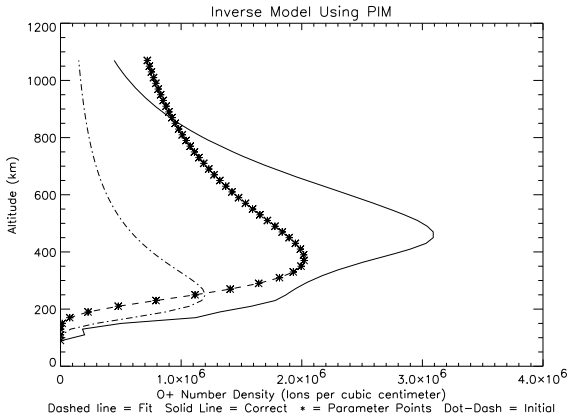

Figure 3.31: Chapman Equation Fitted to PIM Data with Random Noise Set 3

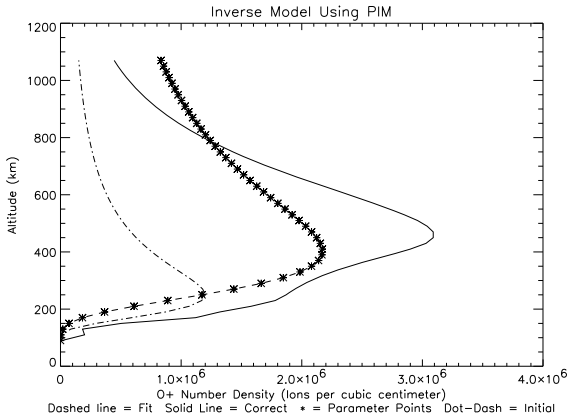

Figure 3.32: Chapman Equation Fitted to PIM Data with Random Noise Set 4

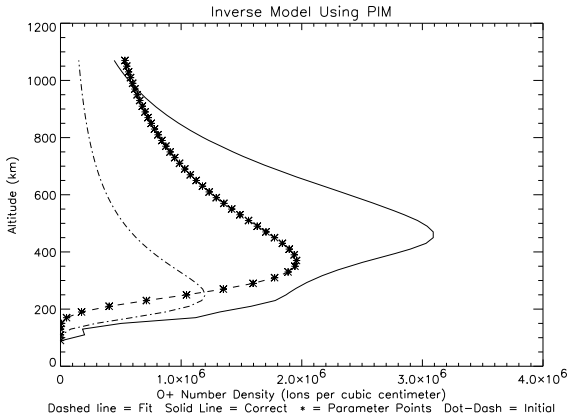

Figure 3.33: Chapman Equation Fitted to PIM Data with Random Noise Set 5

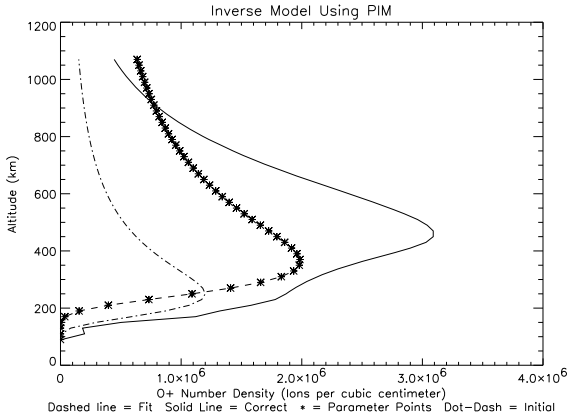

Figure 3.34: Chapman Equation Fitted to PIM Data with Random Noise Set 6

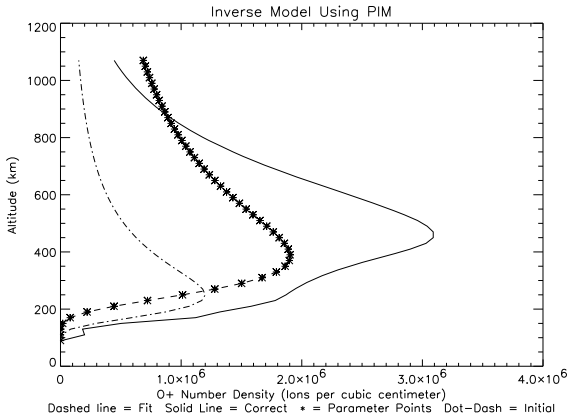

Figure 3.35: Chapman Equation Fitted to PIM Data with Random Noise Set 7

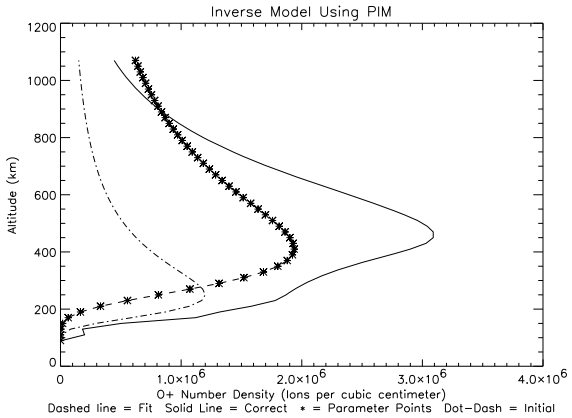

Figure 3.36: Chapman Equation Fitted to PIM Data with Random Noise Set 8

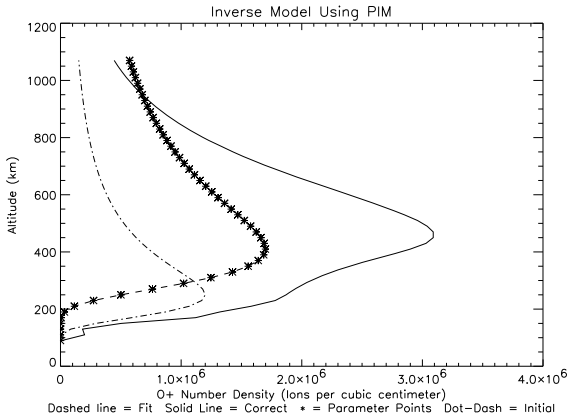

Figure 3.37: Chapman Equation Fitted to PIM Data with Random Noise Set 9

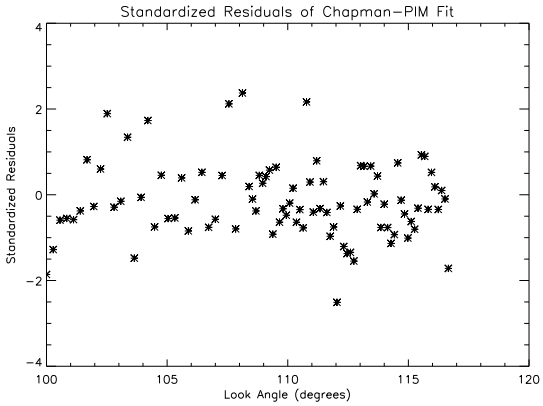

Figure 3.38: Chapman Equation Fitted to PIM Data Standardized Residuals with Random Noise Set 1

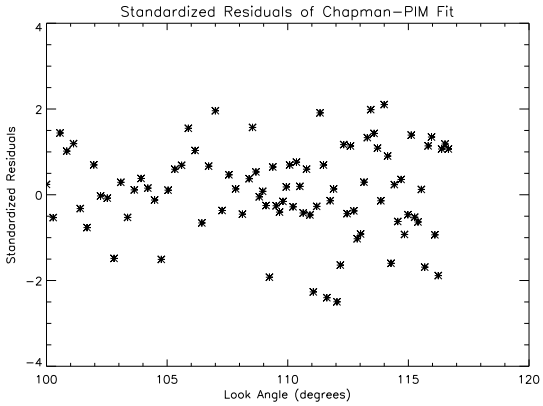

Figure 3.39: Chapman Equation Fitted to PIM Data Standardized Residuals with Random Noise Set 2

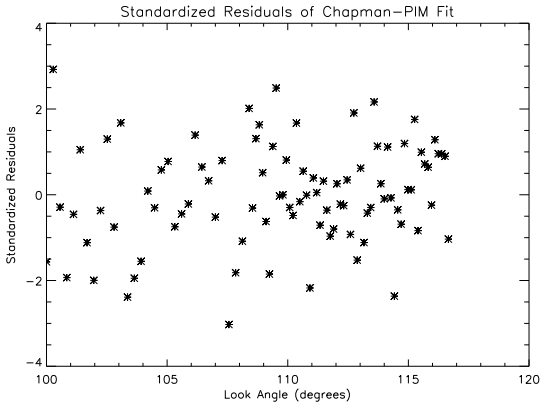

Figure 3.40: Chapman Equation Fitted to PIM Data Standardized Residuals with Random Noise Set 3

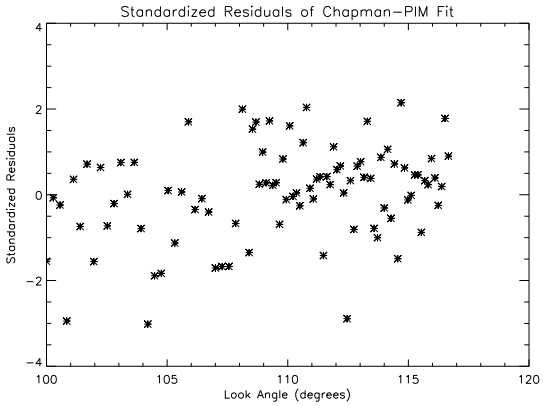

Figure 3.41: Chapman Equation Fitted to PIM Data Standardized Residuals with Random Noise Set 4

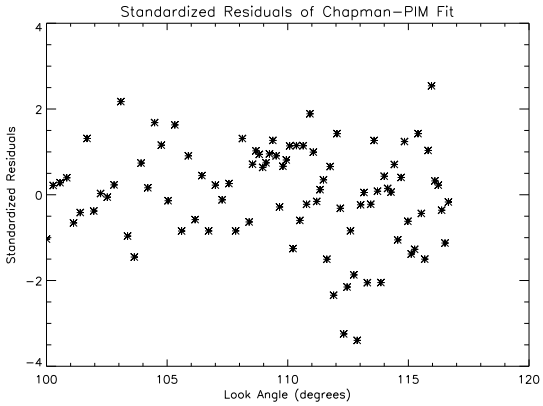

Figure 3.42: Chapman Equation Fitted to PIM Data Standardized Residuals with Random Noise Set 5

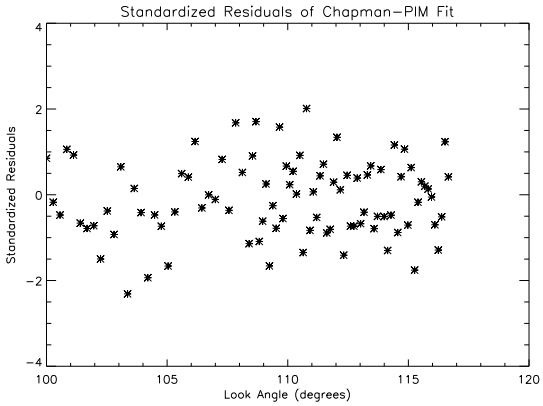

Figure 3.43: Chapman Equation Fitted to PIM Data Standardized Residuals with Random Noise Set 6

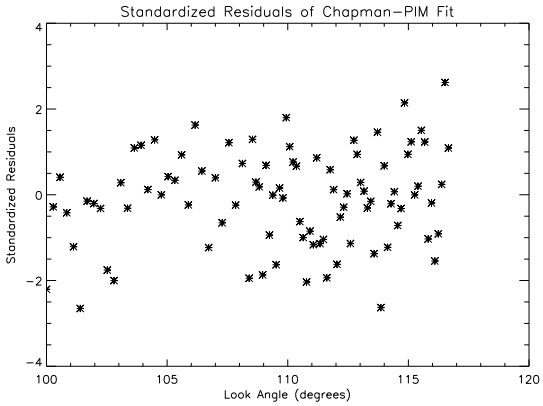

Figure 3.44: Chapman Equation Fitted to PIM Data Standardized Residuals with Random Noise Set 7

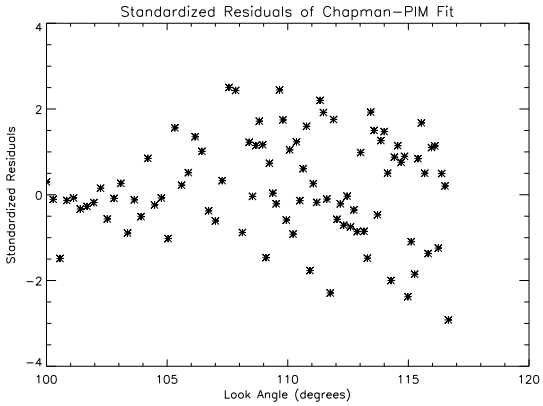

Figure 3.45: Chapman Equation Fitted to PIM Data Standardized Residuals with Random Noise Set 8

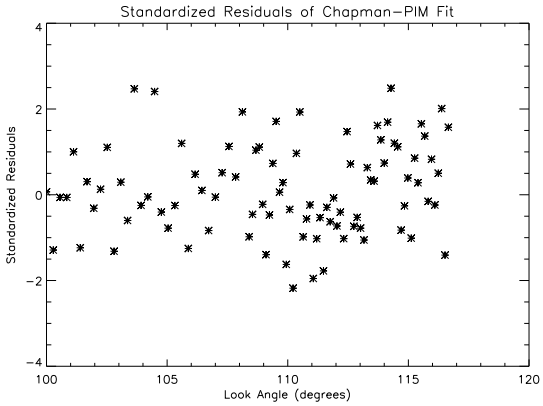

Figure 3.46: Chapman Equation Fitted to PIM Data Standardized Residuals with Random Noise Set 9

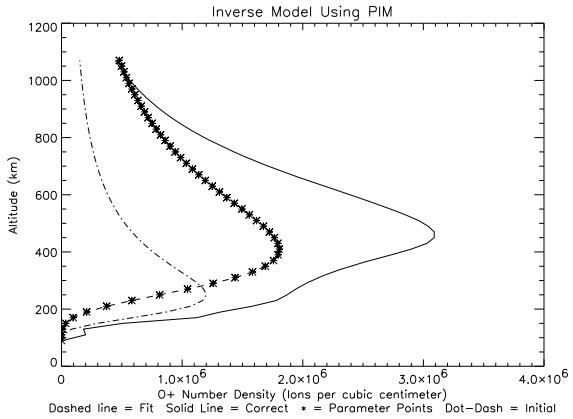

Figure 3.47: Chapman Equation Fitted to PIM Data with 25% Random Noise Set 1

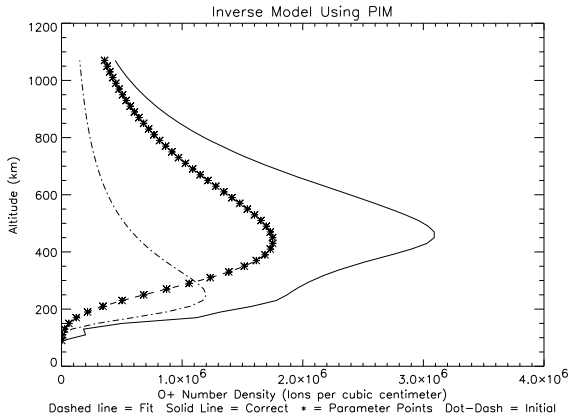

Figure 3.48: Chapman Equation Fitted to PIM Data with 25% Random Noise Set 2

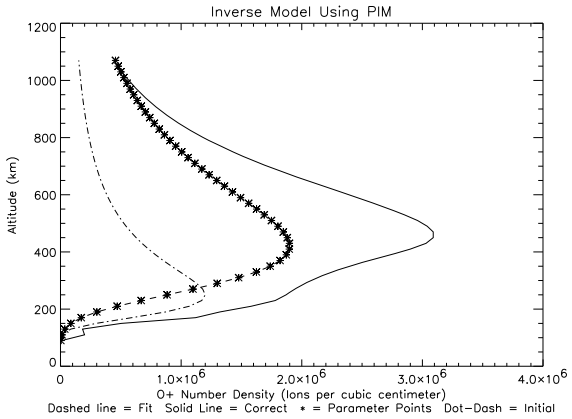

Figure 3.49: Chapman Equation Fitted to PIM Data with 25% Random Noise Set 3

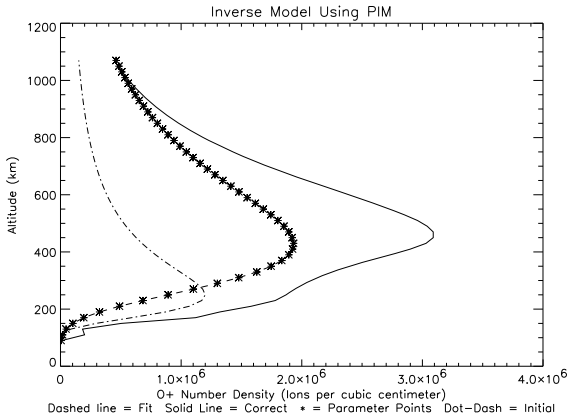

Figure 3.50: Chapman Equation Fitted to PIM Data with 25% Random Noise Set 4

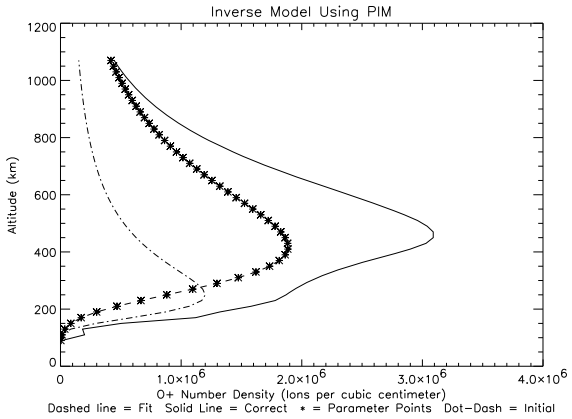

Figure 3.51: Chapman Equation Fitted to PIM Data with 25% Random Noise Set 5

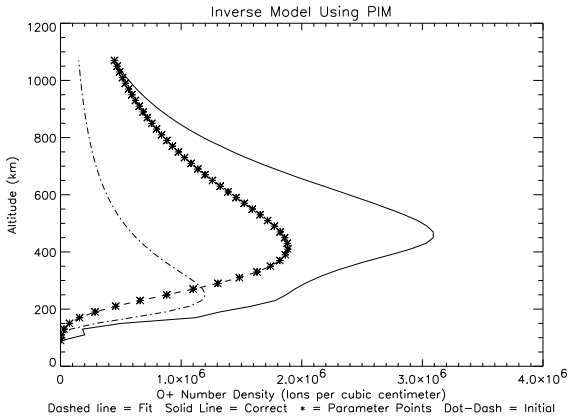

Figure 3.52: Chapman Equation Fitted to PIM Data with 25% Random Noise Set 6

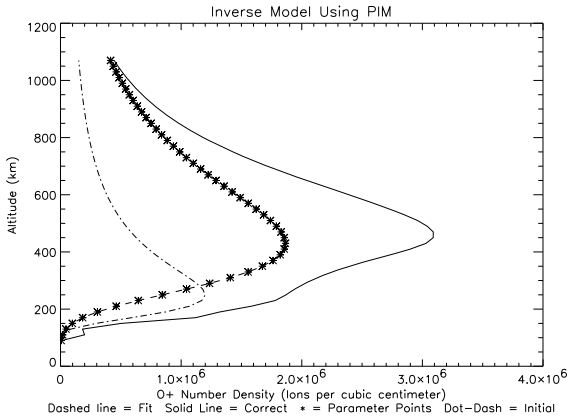

Figure 3.53: Chapman Equation Fitted to PIM Data with 25% Random Noise Set 7

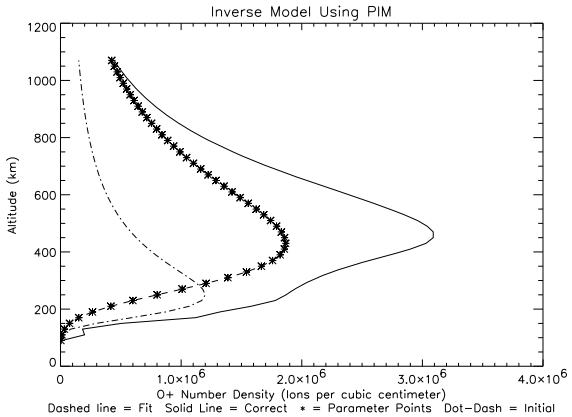

Figure 3.54: Chapman Equation Fitted to PIM Data with 25% Random Noise Set 8

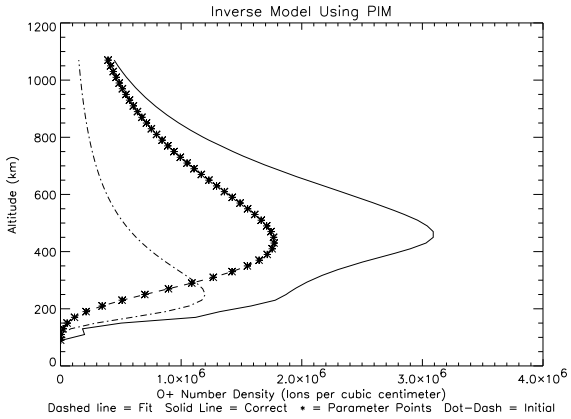

Figure 3.55: Chapman Equation Fitted to PIM Data with 25% Random Noise Set 9

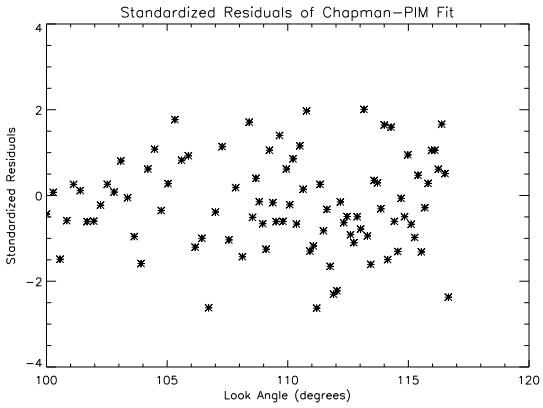

Figure 3.56: Chapman Equation Fitted to PIM Data Standardized Residuals with 25% Random Noise Set 1

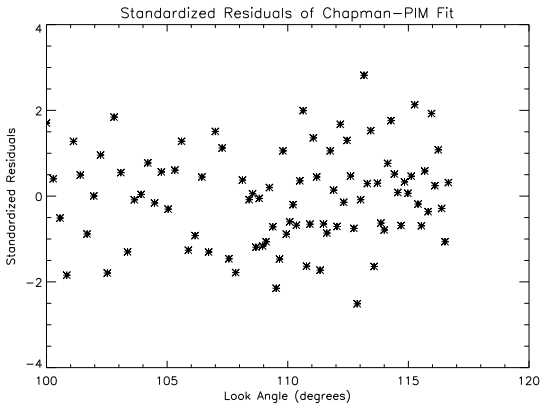

Figure 3.57: Chapman Equation Fitted to PIM Data Standardized Residuals with 25% Random Noise Set 2

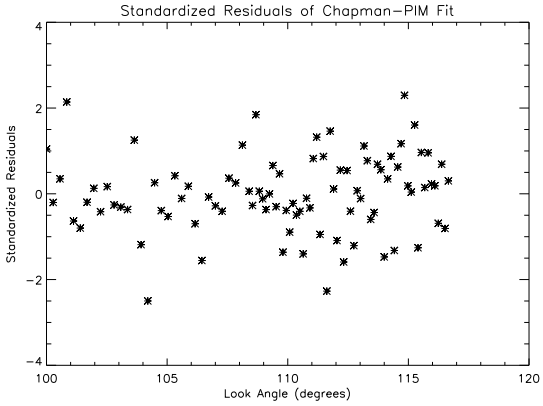

Figure 3.58: Chapman Equation Fitted to PIM Data Standardized Residuals with 25% Random Noise Set 3

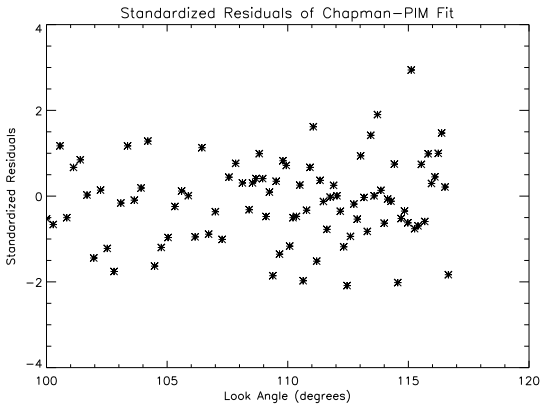

Figure 3.59: Chapman Equation Fitted to PIM Data Standardized Residuals with 25% Random Noise Set 4

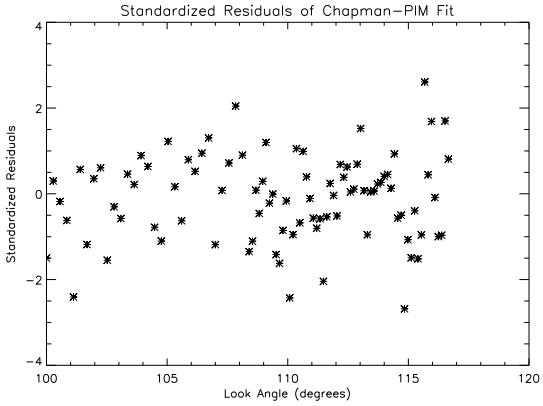

Figure 3.60: Chapman Equation Fitted to PIM Data Standardized Residuals with 25% Random Noise Set 5

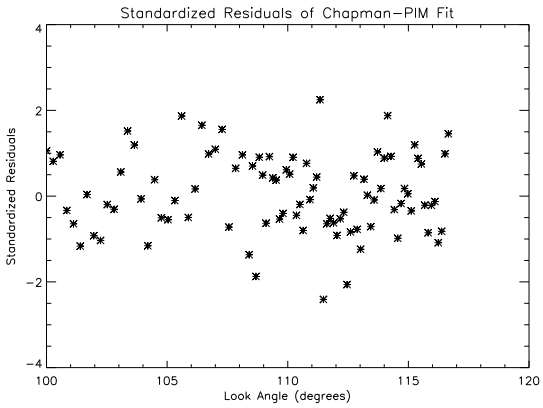

Figure 3.61: Chapman Equation Fitted to PIM Data Standardized Residuals with 25% Random Noise Set 6

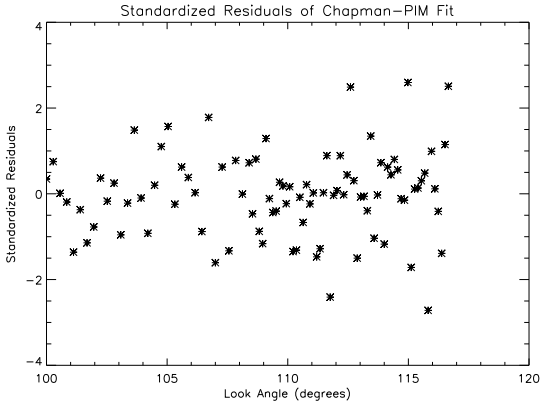

Figure 3.62: Chapman Equation Fitted to PIM Data Standardized Residuals with 25% Random Noise Set 7

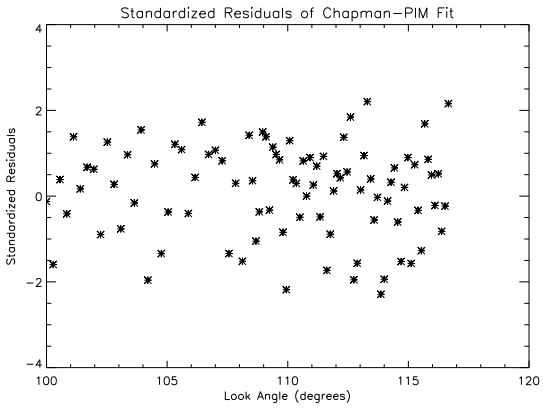

Figure 3.63: Chapman Equation Fitted to PIM Data Standardized Residuals with 25% Random Noise Set 8

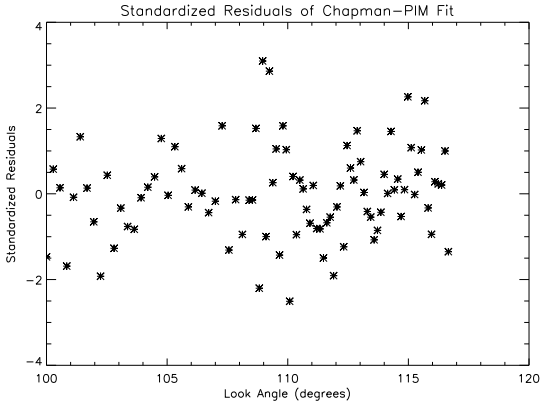

Figure 3.64: Chapman Equation Fitted to PIM Data Standardized Residuals with 25% Random Noise Set 9

Chapter 4

Inverse Model of O^+ Number Density Using a Spline Fit Model

The goal of the spline fit inverse model is to produce an inverse procedure that will model any possible ionospheric O^+ number density profile. The spline fit model does not use the Chapman equation, and is therefore not constrained by its limitations. Any O^+ number density profile can theoretically be modelled, as the parameters of the inverse procedure are points on the profile itself.

We have tested the spline fit model against the same two estimated models that we used to test the Chapman model: the Chapman equation generated profile and the profile generated by PIM. The same noise was added to the 834 Å radiation data to get a true comparison of the two models.

With the spline fit model, we are required to use regularization. The spline fit model can generate a non-smooth model of the O^+ number density profile. This is undesirable, and regularization smooths the profile. Because we use regularization with this model, an appropriate regularization parameter must be found. We must therefore do L-curve analysis on this model.

Because of regularization, we cannot generate covariance or correlation matrices from the $J^T J$ matrix of any significance. The variances established by the covariance matrix would not be the real parameter variance for the establishing of confidence intervals. We have added a parameter that does not apply

equally to these intervals, and any covariance matrix is taking this parameter into account for all its estimates.

We can still use normality tests such as the Anderson-Darling test, χ^2 tests, and residual regression to check the validity of the fit.

4.1 The Spline Fit

We use a spline fit for the new inverse procedure. We use a spline fit of the O^+ profile instead of just using layers because we need 50 layers to generate a reasonable model. By using a spline fit, we generate a parameter set that is nearly as precise, more easily smoothed, and faster to run. In our spline fit model, we chose fifteen of the fifty layers, and spline fit the other layers to end with fifty layers.

To create an accurate spline fit model, we used every other layer near the low end of the F layer of the ionosphere, about every 40 kilometers, starting at 110 kilometers. These close parameters are necessary because the lower end of the F layer has more change over smaller changes in altitude, and the forward model is relatively sensitive to the lower altitudes. After the thirteenth parameter point, at 590 kilometers, we used only every ten layers, or two hundred kilometers. The upper end of the F layer does not change as quickly and the forward model is not as sensitive to changes in the upper tail.

At the ends of the spline fits, it was necessary to add a final arbitrary parameter point to make the tails end where they would end. Without these set spline points, the upper and lower tails could increase. This increase in O^+ number density at the ends of the F layer is not physically reasonable. The lower spline

point was set at 0 kilometers, O^+ number density of 0. The upper spline point was set at 1300 kilometers, with an O^+ number density of 20,000.

Finally, using the spline fit required the transformation of all O^+ number densities to their logarithm before fitting the spline. Fitting the spline without first transforming the number densities often resulted in negative number densities at certain layers as the spline was fit. The cubic polynomial between the two parameter points required the spline curve to dip into negative numbers when decreasing rapidly toward zero at the lower altitudes. A logarithmic spline fit does the same, but the transformation makes negative numbers very small positives. A negative number density is obviously a physical impossibility, so this is an undesirable effect. Negative O^+ number densities result in errors in the forward model.

4.2 Forward Model Using the Spline Fit Model

The spline fit model uses a forward model that is nearly identical to that of the Chapman model. The discrepancy lies at the beginning of the forward model. In the spline fit model, we obviously do not use the Chapman equation. Instead, we must generate a cubic spline between those points on the profile that are used as parameters in the inverse procedure. Once the spline fit is generated and fifty layers of the F layer of the ionosphere have been estimated, the forward model proceeds as it did for the Chapman model.

4.3 Spline Inverse Model Using an Initial Ionospheric Model Estimated from the Chapman Equation

We used the spline inverse model to model the Chapman equation produced model. We produced the L curve that showed us what regularization parameter worked best, as shown in Figure 4.1. The appropriate inverse solutions with respect to these regularization parameters are shown in Figures 4.2-4.6. From Figure 4.1 we can see that the appropiate regularization parameter to use would be 4×10^{-5}. At this point we get the bottom left corner of the L curve. This gives us a best value for χ^2 and the regularization of the fit, so that both are minimized without increasing the other needlessly.

At a regularization parameter of 4×10^{-5}, the χ^2 value is 99.537, and the regularization value is 92.290. The χ^2 value gives us a p-value of .1509, which cannot be rejected. The fit passes the χ^2 test. When we check the fit against the Anderson-Darling normality test, we get a p-value of .395, which is also acceptable. We once again check the 95% confidence intervals of the parameters of a regression fit of the residuals to see if they are significantly different from zero. The confidence interval of the constant parameter of the regression fit is [-.5976,.2876]. This interval contains zero. Thc confidence interval of the x coefficient is [-.0064,.0105], which also includes zero. The parameters of the regression coefficients, therefore, also pass the test for a good fit. Finally, we must look at the standardized residuals of the fit in Figure 4.7 to see if any recognizable patterns occur.

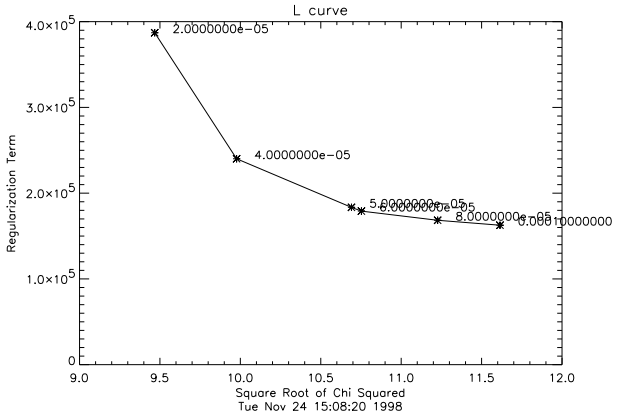

Figure 4.1: L Curve Produced in Generating Fits for the Chapman Equation O^+ Profile

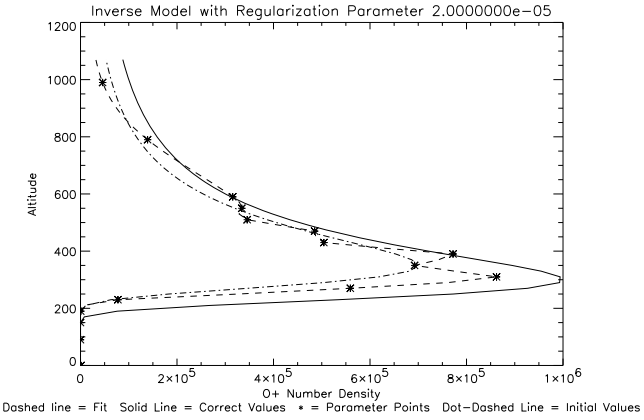

Figure 4.2: Spline Fit of the Chapman Equation Produced O^+ Number Density Profile Using Regularization Parameter 2×10^{-5}

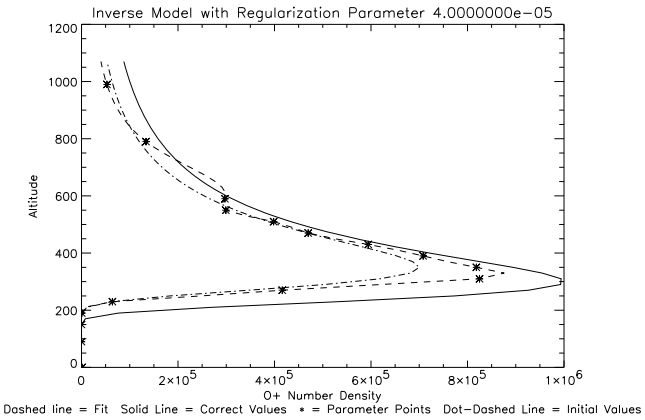

Figure 4.3: Spline Fit of the Chapman Equation Produced O^+ Number Density Profile Using Regularization Parameter 4×10^{-5}

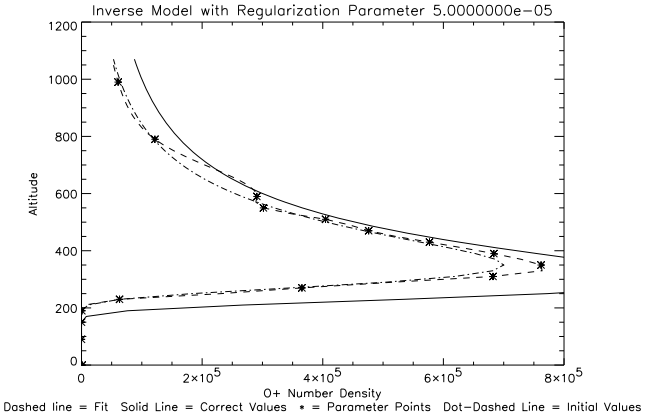

Figure 4.4: Spline Fit of the Chapman Equation Produced O^+ Number Density Profile Using Regularization Parameter 5×10^{-5}

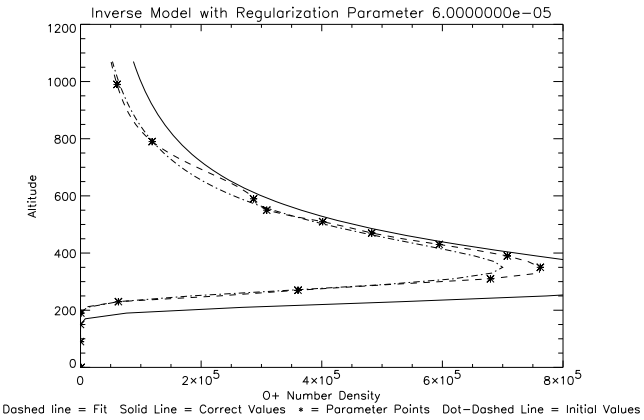

Figure 4.5: Spline Fit of the Chapman Equation Produced O^+ Number Density Profile Using Regularization Parameter 6×10^{-5}

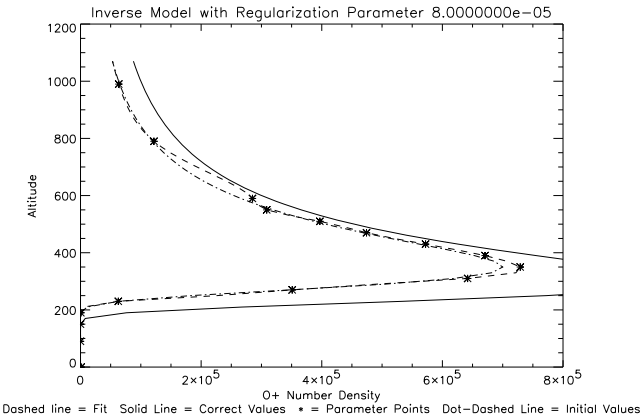

Figure 4.6: Spline Fit of the Chapman Equation Produced O^+ Number Density Profile Using Regularization Parameter 8×10^{-5}

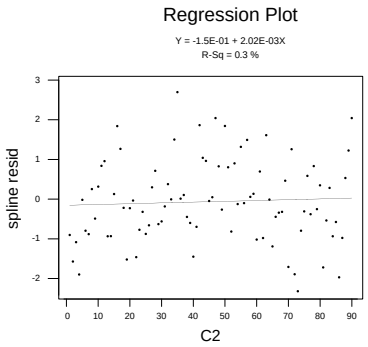

Figure 4.7: Standardized Residuals of the Spline Fit to the Chapman Equation Generated Data Set for Regularization Parameter .00004

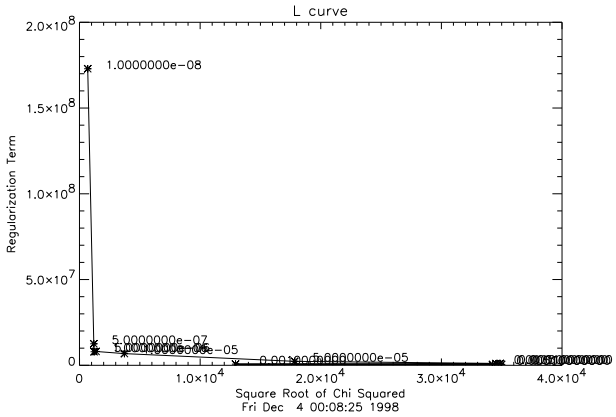

Figure 4.8: L Curve for the Spline Model Fit of PIM Profile

4.4 Spline Inverse Model Using an Initial Ionospheric Model Estimated from PIM

We also attempted to fit the PIM profile with the spline fit inverse model. The results showed that work could be done on the spline fit model. The L curve shown in Figure 4.8 shows the poor fits gotten by this inverse model. Figures 4.9-4.18 show how poorly the fits estimate the profile.

We can evaluate two of the best above models to show that none of these fits is any good at all. Figure 4.9 has the best numbers on the L curve. Both the χ^2 value and regularization value are the lowest of the fits performed. Looking at the figure, it is obvious that the fit is poor. The figure follows no patterns that match the behavior of O^+ ions in the F layer. But even this fit cannot be good fits because Figure 4.9 has a χ^2 value of 1183.3. This χ^2 value gives an effective p value for this model of zero. There is no way that these fits are any good at all.

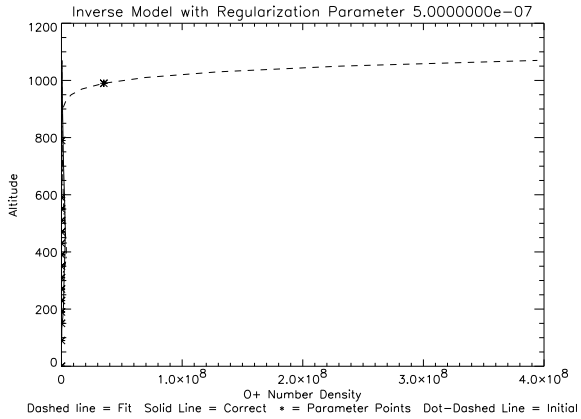

Figure 4.9: Spline Fit of the PIM Profile Using Regularization Parameter .0000005

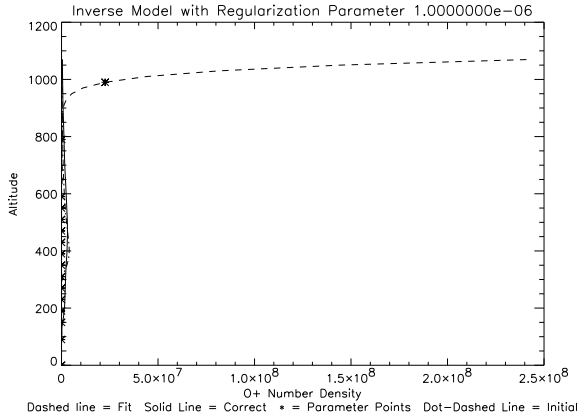

Figure 4.10: Spline Fit of the PIM Profile Using Regularization Parameter .000001

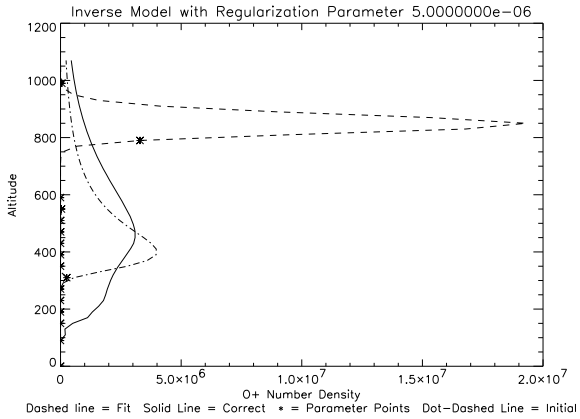

Figure 4.11: Spline Fit of the PIM Profile Using Regularization Parameter .000005

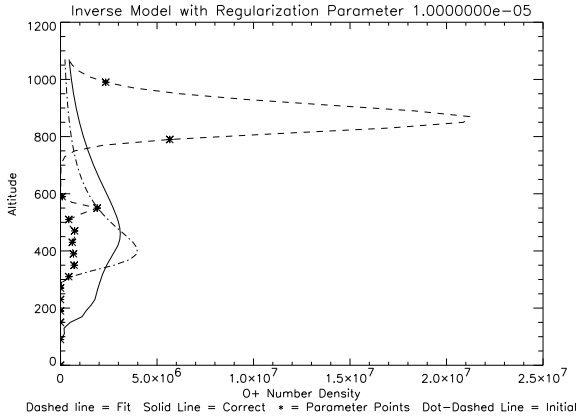

Figure 4.12: Spline Fit of the PIM Profile Using Regularization Parameter .00001

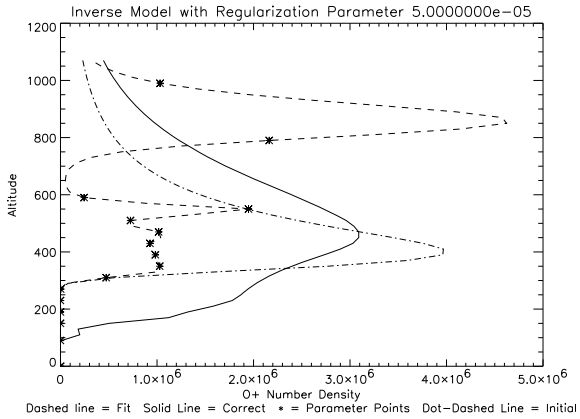

Figure 4.13: Spline Fit of the PIM Profile Using Regularization Parameter .00005

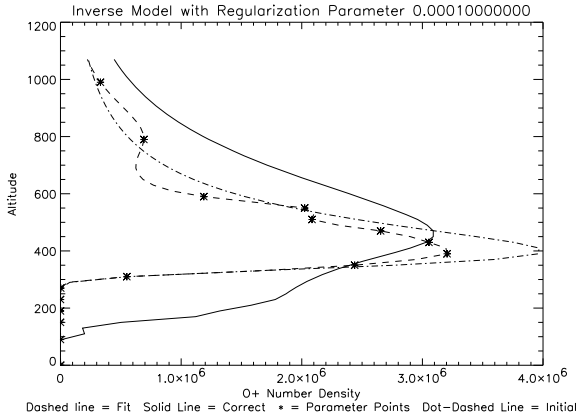

Figure 4.14: Spline Fit of the PIM Profile Using Regularization Parameter .0001

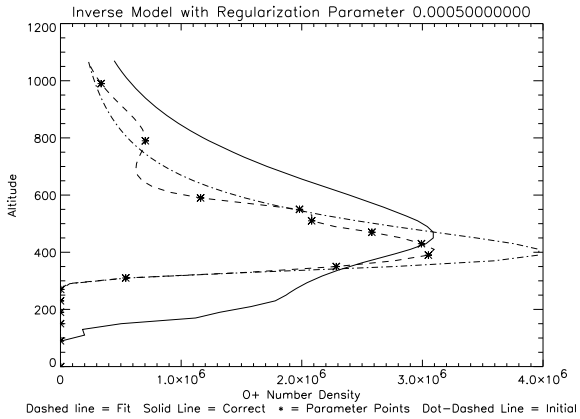

Figure 4.15: Spline Fit of the PIM Profile Using Regularization Parameter .0005

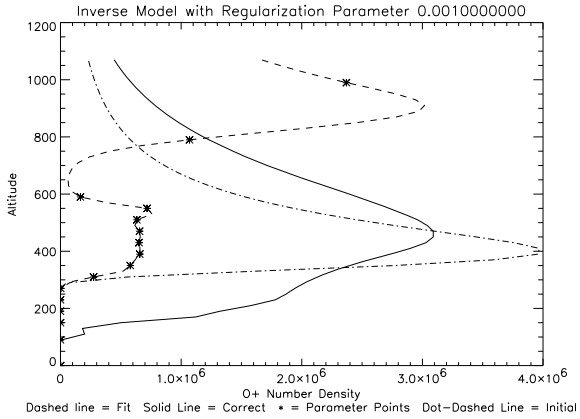

Figure 4.16: Spline Fit of the PIM Profile Using Regularization Parameter .001

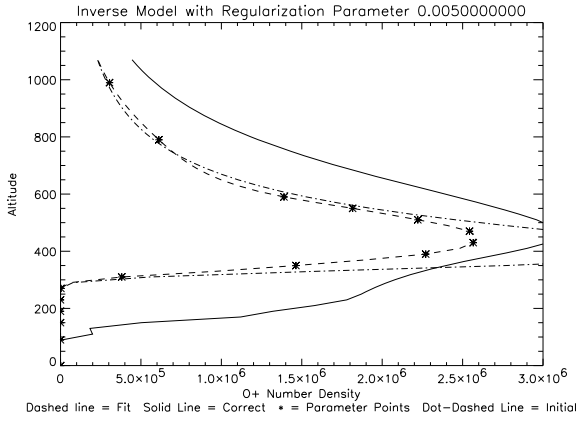

Figure 4.17: Spline Fit of the PIM Profile Using Regularization Parameter .005

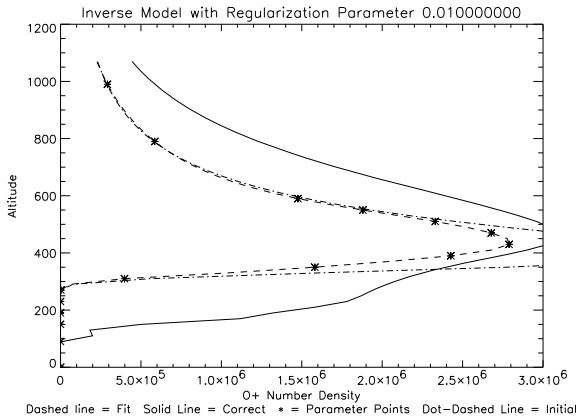

Figure 4.18: Spline Fit of the PIM Profile Using Regularization Parameter .01

Chapter 5

Results and Conclusions

The results of the spline fit model are inconclusive. For the Chapman model, the spline fit model appears to work, approximately as well as the Chapman model. As shown with the PIM model, it does need some work. With more research the spline fit model could be a solution to the problem of modelling ionospheric F layer O^+ number density from 834 Å airglow. The conclusive results of this thesis involve the analysis of fits to data.

After using the Chapman model to form an estimation of the O^+ number density in the ionosphere, we must analyze the results using multiple techniques. The fit could have a very good χ^2 value, but not be a good estimation of the real F layer. We must use supplementary techniques such as the Anderson-Darling normality test, residual regression to check for a good residual fit, and examination of the residuals for strange and unusual patterns suggesting a poor fit. Using these tests, we can sometimes disclude a fit that has a decent χ^2 value because of a failure of the fit in some other way.

If we had more accurate sensors, we could have more information in the determination of whether the fit is good or not. After reducing the noise of the PIM data set by 75%, we showed that nearly twice as many models were poor fits. A better, more accurate sensor could reduce noise and make the process of generating a fit to a data set more reliable.

References

[Anderson and Meyer, 1985] Anderson, D. E. and Meyer, R. R. (1985). The OII 834-Å dayglow: A general model for excitation rate and intensity calculations. *Planetary Space Science*, 33(10):1179–1186.

[Bain and Engelhardt, 1992] Bain, L. J. and Engelhardt, M. (1992). *Introduction to Probability and Mathematical Statistics*. Duxbury Press, Belmont, California, second edition.

[Bard, 1974] Bard, Y. (1974). *Nonlinear Parameter Estimation*. Academic Press, Inc., New York, New York.

[Bevington and Robinson, 1992] Bevington, P. R. and Robinson, D. K. (1992). *Data Reduction and Error Analysis for the Physical Sciences*. WCB/McGraw-Hill, New York, New York, second edition.

[Christiansen et al., 1993] Christiansen, A. B., Kayser, D. C., Pranke, J., Strauss, P. R., Gutierrez, D. J., Chakrabarti, S., McCoy, R. P., Meier, R. R., Wolfram, K. D., and Picone, J. M. (1993). Instrumentation on the remote atmospheric and ionospheric detection system experiment: Extreme ultraviolet spectrometer, photometer, and near-infrared spectrometer. *Optical Engineering*, 32:3054.

[Daniell Jr. et al., 1995] Daniell Jr., R. E., Brown, L. D., Anderson, D. N., Fox, M. W., Doherty, P. H., Decker, D. T., Sojka, J. J., and Schunk, R. W.

(1995). Parameterized ionospheric model: A global ionospheric parameterization based on first principles models. *Radio Science*, 30(5):1499–1510.

[D'Augostino and Stevens, 1986] D'Augostino, R. B. and Stevens, M. A., editors (1986). *Goodness of Fit Techniques.* Mercel Dekkar, New York, New York.

[Gill et al., 1981] Gill, P. E., Murray, W., and Wright, M. H. (1981). *Practical Optimization.* Academic Press, Inc., San Diego, California.

[Hansen, 1992] Hansen, P. C. (1992). *Regularization Tools: A Matlab Package for Analysis and Solution of Discrete Ill-Posed Problems.* Danish Computing Center for Research and Education, Building 305, Technical University of Denmark, DK-2800 Lyngby, Denmark, 3.0 edition. Revised March 1998.

[Hedin, 1987] Hedin, A. E. (1987). MSIS-86 thermospheric model. *Journal of Geophysical Research*, 92(A5):4649–4662.

[Lawson and Hanson, 1974] Lawson, C. L. and Hanson, R. J. (1974). *Solving Least Squares Problems.* Prentice-Hall, Englewood Cliffs, New Jersey.

[Levenberg, 1944] Levenberg, K. (1944). A method for the solution of certain non-linear problems in least squares. *Quarterly of Applied Mathematics*, 2:164–168.

[Marquardt, 1963] Marquardt, D. W. (1963). An algorithm for least-squares estimation of nonlinear parameters. *SIAM Journal of Applied Mathematics*, 11(2):431–441.

[McCoy et al., 1985] McCoy, R. P., D. E. Anderson, J., and Chakrabarti, S. (1985). F_2 region ion densities from analysis of O^+ 834-Å airglow: A parametric study with comparisons with satellite data. *Journal of Geophysical Research*, 90(A12):12257–12264.

[McCoy et al., 1994] McCoy, R. P., Dymond, K. F., Fritz, G. G., Thonnard, S. E., Meier, R. R., and Regeon, P. A. (1994). Special sensor ultraviolet limb imager: An ionospheric and neutral density profiler for the Defense Meteorological Satellite Program satellites. *Optical Engineering*, 33:423.

[Parker, 1994] Parker, R. L. (1994). *Geophysical Inverse Theory.* Princeton University Press, Princeton, New Jersey.

[Picone et al., 1997] Picone, J. M., Meier, R. R., Kelley, O. A., Dymond, K. F., Thomas, R. J., Melendez-Alvira, D. J., and McCoy, R. P. (1997). Investigation of ionospheric O^+ remote sensing using the 834-$\mathring{A}$ airglow. *Journal of Geophysical Research*, 102(A2):2441–2456.

[Ramsey and Schafer, 1997] Ramsey, F. L. and Schafer, D. W. (1997). *The Statistical Sleuth: A Course in Methods of Data Analysis.* Duxbury Press, Belmont, California.

[Tikhonov and Arsenin, 1977] Tikhonov, A. N. and Arsenin, V. Y. (1977). *Solutions of Ill-Posed Problems.* John Wiley, New York, New York.

[Tikhonov et al., 1995] Tikhonov, A. N., Goncharsky, A. V., Stepanov, V. V., and Yagola, A. G. (1995). *Numerical Methods for the Solution of Ill-Posed Problems.* Kluwer Academic Publishers, Dordrecht, The Netherlands. Originally published in Moscow, U.S.S.R. in 1990.

[Twomey, 1977] Twomey, S. (1977). *Introduction to the Mathematics of Inversion in Remote Sensing and Indirect Mesurements*. Dover Publications, Inc., Mineola, New York.

This thesis is accepted on behalf of the faculty of the Institute by the following committee:

Advisor

Date